Savannah River National Laboratory™

OPERATED BY SAVANNAH RIVER NUCLEAR SOLUTIONS

2013 Savannah River National Laboratory LDRD Annual Report



Table of Contents

A strong Laboratory Directed Research and Development (LDRD) program is a cornerstone of the work of a National Laboratory. I am pleased that at SRNL, the LDRD program is continuing to grow, to thrive, and to further enable us to demonstrate the quality of SRNL's research.

This report demonstrates the execution of our LDRD program within the objectives and guidelines outlined by the Department of Energy (DOE) through the DOE Order 413.2b. The projects described within the report align purposefully with SRNL's strategic vision and provide great value to the DOE. The diversity exhibited in the research and development projects underscores the DOE Office of Environmental Management (DOE-EM) mission and enhances that mission by developing the technical capabilities and human capital necessary to support future DOE-EM national needs. As a multiprogram national laboratory, SRNL is applying those capabilities to achieve tangible results for the nation in National Security, Environmental Stewardship, Clean Energy and Nuclear Materials Management.

On behalf of the SRNL Management team, I would like to thank those members of the SRNL staff, and their research partners, for their accomplishments and the quality of their work. Because of their efforts, the LDRD program will continue to be a critical mechanism to demonstrate why SRNL's competencies are important to the nation.

Terry Michalske
Laboratory Director, SRNL

Overview of 2013 Laboratory Directed Research and Development Program

The Laboratory Directed Research and Development (LDRD) Program at Savannah River National Laboratory (SRNL) supports high quality research and development to further the mission of the Department of Energy. Research teams supported through LDRD in FY13 yielded quality research in a variety of technical focus areas. The high-risk, potentially high-value, research supported under the LDRD program fosters inventiveness and inspires study at the forefront of science and technology. Laboratory researchers form technical teams both within the laboratory, as well as externally with the commercial sector, university professors, post-doctoral researchers and students to tackle common technical goals. Technical expertise is exchanged and new ideas developed through the technical discussions and interactions supported by the program.

Tangible accomplishments resulting from persistent technical efforts in FY13 include:

Scientific Productivity

Research efforts supported by the LDRD program led to securing intellectual property. Six invention disclosures were submitted related to research supported through the LDRD program in FY13. Two patent applications were granted in FY13, including:

- *Novel Method for Synthesizing Alane without the Formation of Adducts and Free of Halide (US Patent 8,377,415 B2)*
- *Use of Titanium-based Materials as Bactericides (US Patent 8,545,820)*

Post-Doctoral and Student Involvement

- Seven post-doctoral researchers were members of 11 LDRD supported research teams in FY13, six performed research at SRNL.
- Four LDRD projects supported graduate student involvement in FY13. Two projects supported undergraduate participation.

Characterization of Chemical Changes Observed for Uranium and Plutonium Particulate Materials

NJ Bridges, GA Fugate, MR Kriz, JJ Pittman, MJ Siegfried, MS Wellons

Small uranium and plutonium particulates emanating from nuclear fuel cycle and weaponization processes can be collected at significant distances from their source. The chemical and physical characteristics of these particles will depend on the production environment while their stability is determined by internal reactions with themselves, other environmental conditions and matrices which they settle on. Therefore, a greater understanding of dispersed uranium and plutonium bearing particulate chemistry will allow more accurate fate and transport models, enhanced design of collection systems, and improved analytical characterization methodologies.

The objective of this research is to gain a fundamental understanding of the species formed when a variety of known uranium and plutonium particulate materials are exposed to environmental stresses. Work performed within FY13 built on the experiments performed in FY12 and examined aerosol production using sonic atomization to perform an in depth examination of the formation of uranyl nitrate particulates, including a few non aqueous studies. Additional work examined production of other uranium salts and scoping studies into production of plutonium materials. Accomplishments of the two year study included, development of a SRNL aerosol generation test bed and the establishment of the corresponding institutional knowledge, and several publications in preparation on uranium aerosol generation and characterization. It is anticipated that the uranium aerosol generation devices built within this project will continue to support and expand current and future DOE-NNSA and WFO projects.

As in FY12, samples were collected passively on a variety of substrates and actively, when analytical techniques required production of a higher sample load. A variety of substrates were employed based on reactivity and analyses concerns. After production, representative samples were stored under a variety of relative humidity (RH) conditions and analyzed periodically over the course of weeks to months. These samples, after being exposed to environmental stresses, demonstrated changes in chemical species and were characterized via Raman spectroscopy and, electron and X-ray diffraction techniques.

The chemical nature of the particulate material was analyzed using Raman spectroscopy to study the chemical species present in the sample. In particular the uranyl bond is a useful probe for spectroscopic techniques, being sensitive to the coordination environment around the uranyl species. The particle morphologies for low level uranium particulates can be examined directly by Scanning Electron Microscopy (SEM) and, as appropriate for smaller particles, Transmission Electron Microscopy (TEM). SEM images were collected using an almost unique instrument that combines the capability of doing high resolution SEM, elemental analysis using a large area Energy Dispersive Spectroscopy (EDS), and *in situ* Raman spectroscopy. TEM grids were deployed as passive substrates for collection of particles and submitted for TEM analysis of low level uranium at Clemson University and macroscopic crystal properties were determined using powder X-ray diffraction (pXRD. Additional studies have been performed in collaboration with the University of South Carolina Aiken to examine potential enhanced particulate characterization using surface enhanced Raman substrates.

Initial experiments were performed with plutonium (IV) nitrate solutions in nitric acid with excess acid required to maintain the solubility of the plutonium. Particulates were generated within a specialty test bed located in a radiation area and several scoping studies were performed with subsequent analyses by SEM, pXRD and Raman. This resultant material was not crystalline and instead formed an amorphous film, which is likely a result of the dilute Pu concentration in the aerosolize droplets. Based on experience with uranium and difficulty in performing plutonium work from both radiological and solubility standpoints, these studies were abandoned. Sonic atomization is likely not an appropriate formation mechanism for these materials. However, these studies resulted in the development of a low cost sample holder that allows for Raman spectroscopy to be performed on plutonium samples outside of radiological control areas.

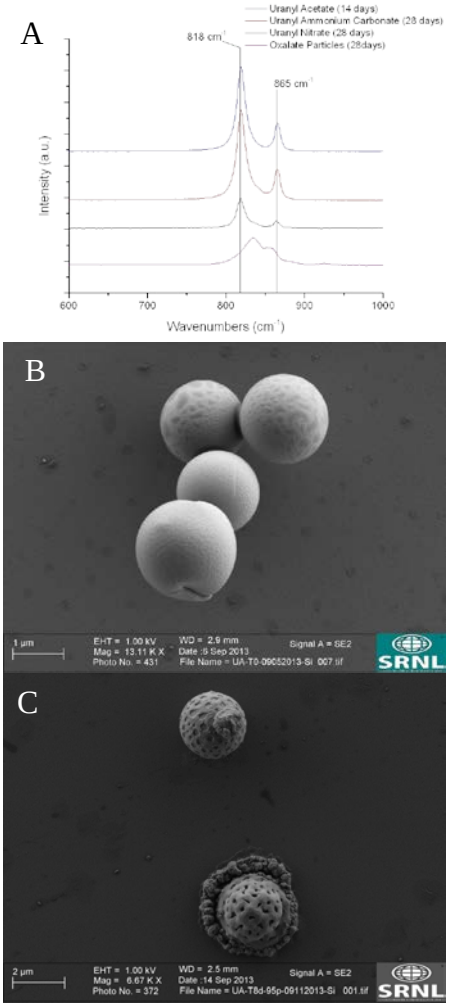

Figure 1. A) Raman spectra for various species after aging. B) Initial morphology of uranyl acetate particles. C) Morphology changes of uranyl acetate particles after 8 day 95% RH sample.

Additional studies with other, more strongly complexing uranyl compounds produced concerted spherical dry particulates. This is suggestive than more strongly binding ligands or the ability to displace additional water from the inner hydration sphere may lead to the formation of drier particulates than the previously studies nitrate system.

Figure 1A suggests that the acetate and carbonate system have transitioned to similar end states as was observed with nitrate, reacting to form the peroxy species studtite. Figure 1B and C shows typical changes in morphology observed for the acetate system. It is unclear at this time whether the oxalate system is also undergoing the same transition, albeit much more slowly, or if it is progressing to another end state. Additional longer term aging studies may suggest that oxalate is transitioning to a different end product, likely a combined species including both an oxalate ligand and an oxy/hydroxy species.

The product from nitrate, acetate, and ammonium carbonate uranyl starting materials appear to transition to the same terminal chemical species over time. It is believed that the species is formed by reaction of the free uranyl moiety with peroxide formed by the sonic nebulizer system. Uranyl nitrate and acetate appear to have similar products as both are relatively weak in complexing uranyl. Carbonate is more stable but the formation of peroxide is likely associated with the production of acidic protons (either in reduction of water or in the coordination of hydrogen peroxide with the uranyl) which would destabilize the carbonate complex, resulting in decomposition of carbonate into carbon dioxide and water. Oxalic acid forms the most stable complex from these ligands and is less likely to be destabilized by added protons due to the bidentate nature of the complex. This suggests that the oxalate system may be undergoing the same transition but at a much slower rate or that this system may have exceeded some critical complex stability and be forming and be forming a non-studtite species. Raman spectroscopy suggests that there is still oxalate present in

this species, implying that it has formed a mixed ligand species containing oxalate and potentially oxide or peroxide.

Hardware in the Loop Electrical Grid Simulator

J. V. Cordaro, Chip Fisher

While there are numerous locations that can model and perform grid simulation, the combination of actual electrical hardware and grid simulation with Hardware-in-the-Loop (HIL) capability is rare. By having HIL capability, high voltage and high current switchgear can be tested and models can be generated to duplicate actual performance. With the modernization of the US electrical grid, high accuracy current measurements are essential at key power distribution points. The Savannah River National Laboratory (SRNL) has the nation's only High Current Calibration Laboratory (HCCL). With high current standards originally from NIST, the HCCL is a national asset. Models are needed of the precision current sensors used in the HCCL and how their performance compares to commercial current sensors used on the grid. The HCCL is needed to support the calibration of high current shunts used during the pinch welding of Tritium reservoirs for the US Nuclear Stockpile.

The objective of this research is to build and validate high frequency models of the NIST fabricated Rogowski coils located in the HCCL and compare performance to commercial Current Transformers (CT). Currents from hundreds of amps to 50,000 Amps will be applied to the sensors in series with high speed data capture. Frequencies ranging from DC to 2 KHz will be generated. The effects of adding multiple conductors through a CT to simulate high currents will be evaluated and compared to single conduction measurements. Based on actual data, models will be validated using a Real Time Digital Simulator (RTDS). This project supports SRNL's involvement in the 15 Mega Watt Electrical Grid Simulation Laboratory being built at the Clemson University Restoration Institute located in Charleston SC. This lab will be the highest power grid simulation laboratory in the world.

During 2012, a state-of-the-art RTDS was selected, specified and purchased. The RTDS was installed in the SRNL HCCL. Acceptance and startup testing of the RTDS was completed. SRNL researchers completed training building custom models of electrical components using the RTDS software. Testing was completed using single analog output/inputs and capture using on the RTDS. SRNL researches completed literature searches and selected the highest accuracy CT's for evaluation. Three 10,000 Amp CT were purchased from Zimmer in Germany and received. Due to the potentially high magnetic fields that can be generated in the HCCL, a detailed hazardous analysis was completed and approved clearing the way for research to begin. Additional power amplifiers were installed in the HCCL to reach 1000 Amps continuous output.

Figure 1 shows the connection of the two NIST Rogowski coils installed in a custom Faraday Cage being fed current from a pulse 100,000 Amp transformer. The analog outputs from the Rogowski coils are connected to integration and a high speed data acquisition system. This setup allows simultaneous high speed capture of the two NIST coils allowing inter-comparison data.

Figure 2 shows the connection of the Rogowski coils being fed from a series of high current amplifiers that can provide continuous 1000 Amps from DC up to a frequency of 2 KHz.

Figure 3 shows how using the RTDS, time synchronized pulses can be generated driving the high current transformer feeding current through the Rogowski coils with the output of the coils connected back into the RTDS.

Figure 1: High Current 100,000 Amp transformer with Faraday Cage and Rogowski Coils

Figure 2: 1000 Amp Continuous Power Amplifiers with DC to 2 KHz Response

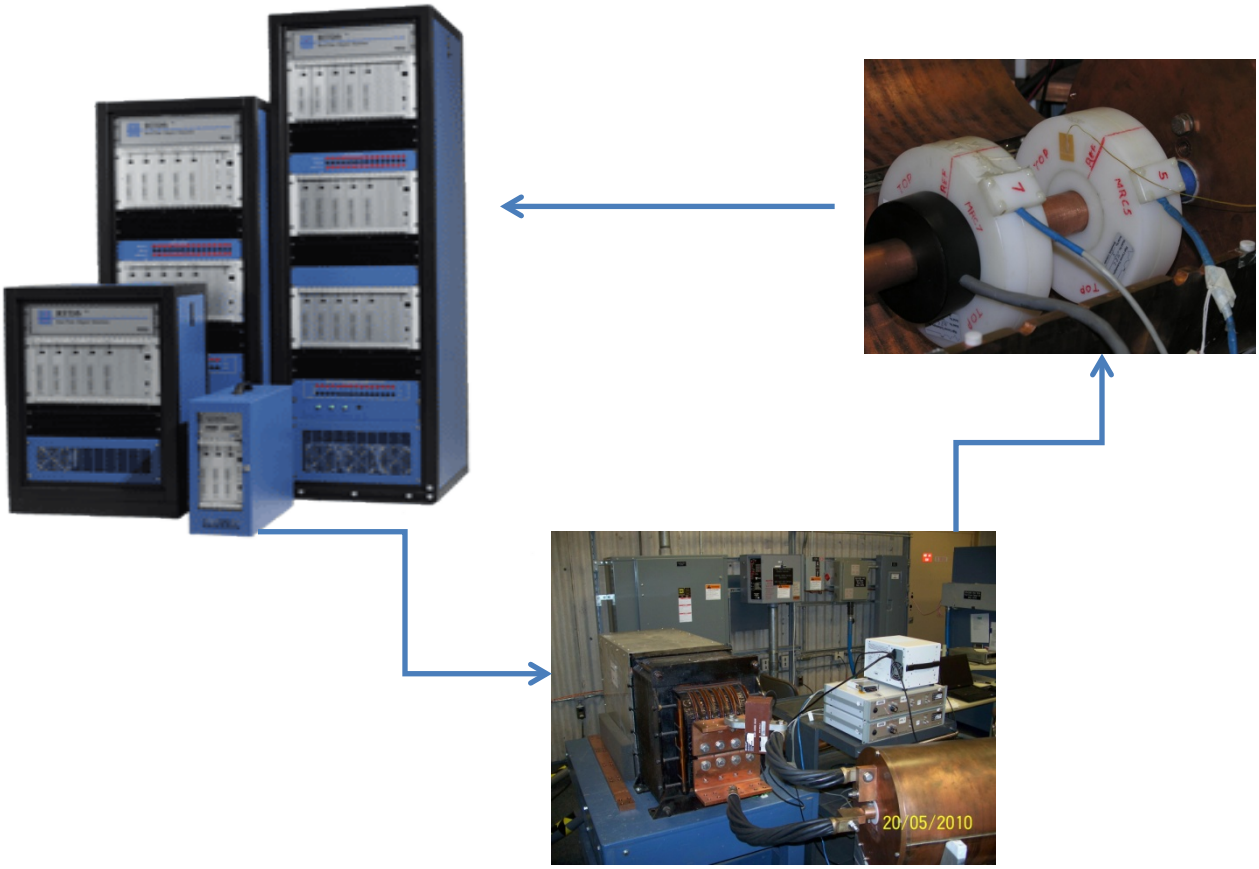

Figure 3: Hardware-In-the-Loop Connection with a RTDS

In FY2013, the highest accuracy commercial CT was purchased and installed in a loop with the SRNL standards. Figure 4 shows the test setup. A custom copper bus bar and fixture was fabricated to allow current up to 1000 Amps continuous be driven through the two current sensors simultaneously.

Figure 4: Commercial CT in Series with SRNL Standard

The first sensor is the SRNL standard from NIST. The second is a 10,000 Amp commercial standard widely used in substations and on the US Electrical Grid. Magnetic field measurements were made to ensure compliance with OSHA standards and a detailed hazard analysis completed prior to running any tests.

MODEL DEVELOPMENT AND TESTING

The RTDS software includes models for 1000's of devices that allow the design of complex grids. Using the models SRNL developed for the commercial high current CT's, equipment manufacturers and power companies can utilize the data and models created to better understand the performance of the CT's under actual condition on the nations electrical grid. An RTDS model was created to generate currents at up to 1000 Amps from DC to 1 KHz. The model, shown in Figure 5, is designed to drive Sine Waves, Triangular Waves and Square Waves.

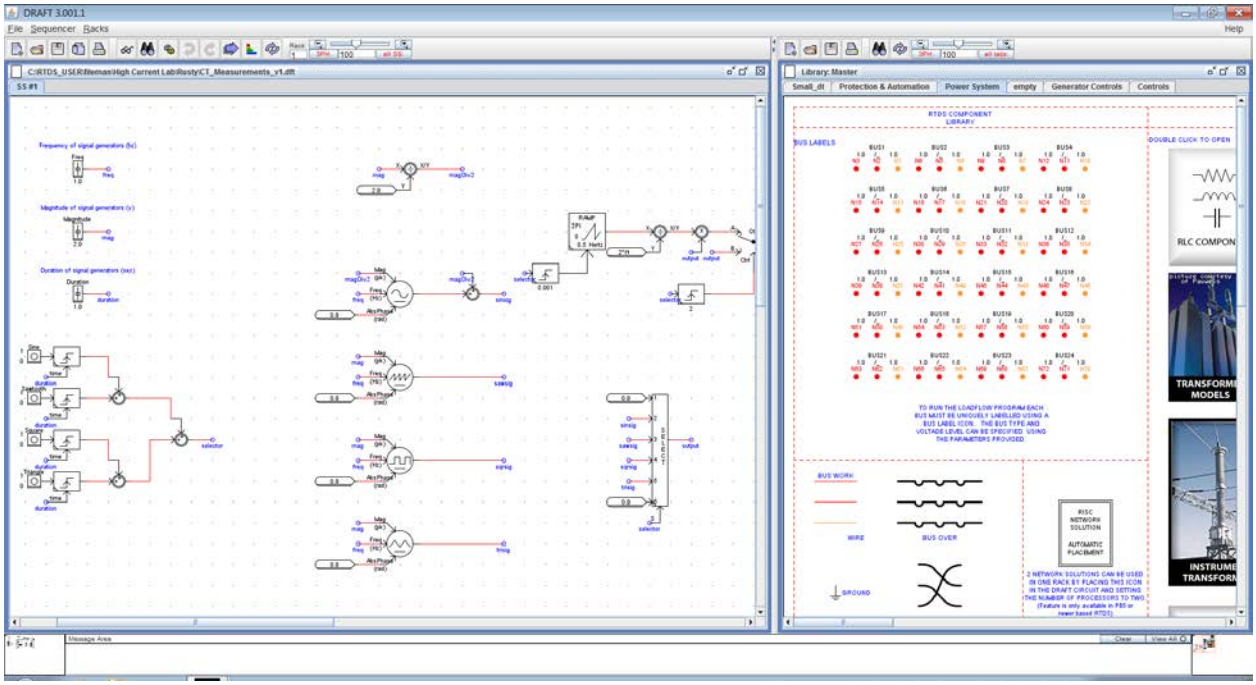

Figure 5: RTDS Model for Driving Current Transformers

The RTDS model included the capability to capture the time synchronized outputs of the two current sensors for a real time comparison. Figure 6 shows the current vs. time plots of the two sensors. The top graph is a raw voltage output that has not been corrected with calibration coefficients. The bottom plot has been corrected. Note that there is a large spike on both CT when the current is turned on. It takes about 6 seconds for the CT's to stabilize. Initial results indicated a significant discrepancies between the SRNL standard and vendor CT. The discrepancy was caused not by the sensors, but the signal conditioning instrumentation. With this data, the models can be adjusted to compensate for the rise time effect.

Figure 6: Comparison of SRNL Standard and Commercial CT

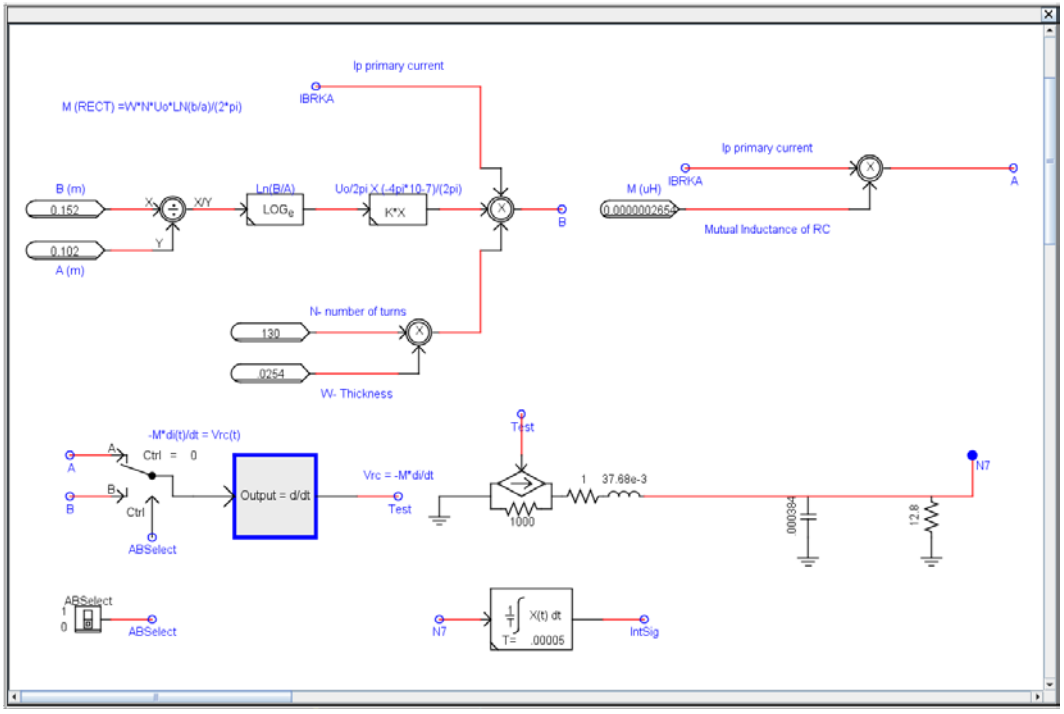

Figure 7: RTDS Rogowski Model

Figure 7 shows the mathematical equivalent of a Rogowski coil using the RTDS modeling software. This model can be adjusted for any Rogowski coil by modifying model parameters based on the actual performance of the coil.

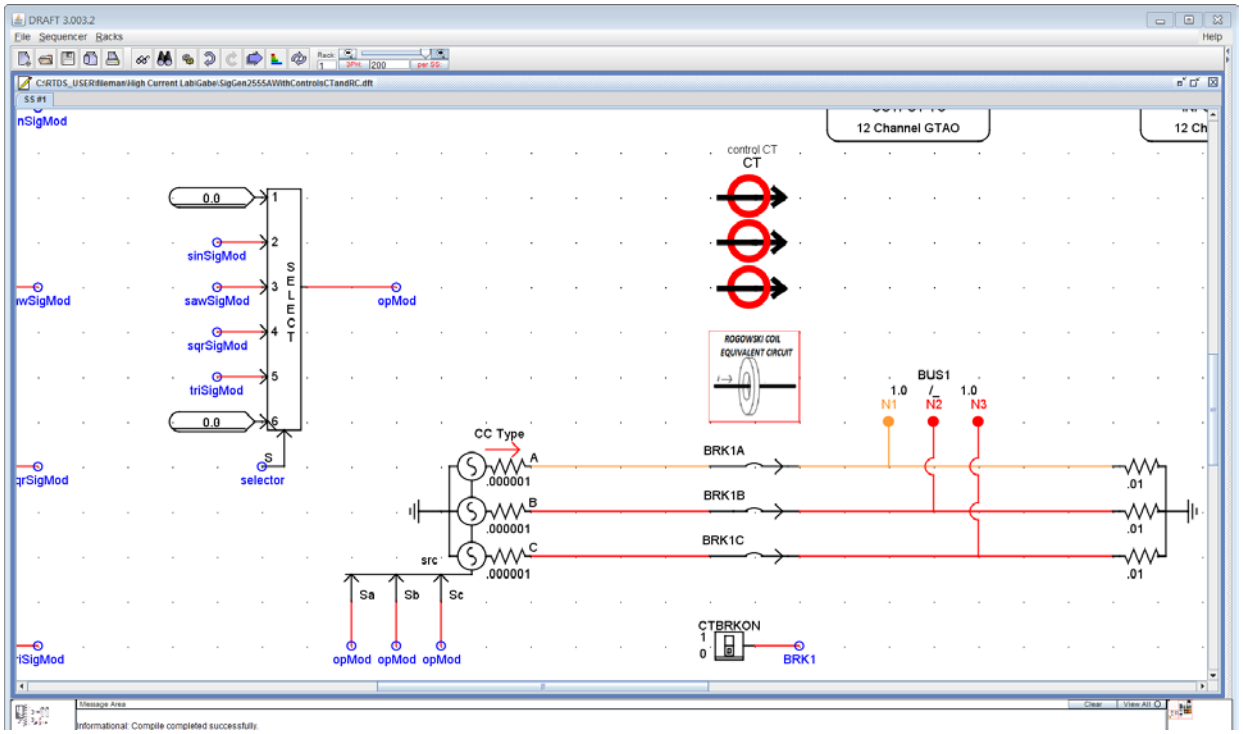

Figure 8: Three Phase Network with Rogowski Model

Figure 8 illustrates how the Rogowski Coil model can be incorporated into a 3 phase power system from a utility substation or power plant. The utility can modify the voltage and frequency level and obtain a real time 3 phase current output.

SUMMARY

As a result of this LDRD project, SRNL now has the capability to calibrate, model and validate high current sensors used by substations and on the US electrical grid. This capability, with the US high current standards is unique in the US. SRNL is now positioned to fill a gap for the DOE as well as the US power producers. Combined with the ISO17025 Standards Laboratory, SRNL can provide high voltage, high current and power calibrations.

Non-Aqueous Electrochemical Fluorination of Used Nuclear Fuel as an Advanced Separation Process

B. L. Garcia-Diaz, L. Olson, M. J. Martinez-Rodriguez, D. Click, and J. Gray

The development of efficient and environmentally benign methods to reprocess used nuclear fuel (UNF) will be enabling technologies for the nuclear renaissance. Non-aqueous methods of fuel processing are currently being developed to reprocess UNF with significantly reduced waste volumes. An electrochemical fluorination process is being developed that is capable of efficiently separating gas phase uranium through potential control of the reaction. Thermodynamic modeling has shown that a galvanic reaction between UNF and a fluorinating agent such as NF_3 in a molten fluoride electrolyte is possible and could selectively fluorinate U to UF_6. Reactor and separation systems have been developed to prove this concept experimentally.

The use of electrochemical and fluorination methods for reprocessing UNF and been proposed and researched by various groups, but combinations of electrochemical and fluorination methods have not been investigated. Fluorinating agents are extremely potent oxidizing agents and should be able to electrochemically fluorinate metallic UNF with no input of electricity. The technical object of this project is to demonstrate the thermodynamic feasibility of electrochemical fluorination for UNF separations, demonstrate the electrochemical fluorination process, and develop flowsheets to show how this technique can be incorporated into state-of-the-art reprocessing schemes.

Thermodynamic calculations of half-cell potentials for potential electrochemical reactions for all UNF constituents were performed using HSC Chemistry. The analysis normalized the potentials against a Ni/NiF_2 reference that is used for many molten fluoride electrochemical cells. Thermodynamic analysis was conducted at temperatures between 0°C and 800°C. Operation is anticipated to be best in the range of 500-600°C with a eutectic mixture of LiF-NaF-KF (FLiNaK) to keep corrosion reactions to a minimum. The electrochemical reactor consists of a glassy carbon crucible to hold the molten salt and glassy carbon porous cathode for NF_3 reduction. An engineering drawing for the reactor is shown in Figure 1. Depleted uranium (DU) turnings are used as surrogate material for UNF to prove the evolution of UF_6. Thermodynamic calculations have also been performed to demonstrate the feasibility of reduction of oxide UNF fuel to its metallic state using HSC chemistry.

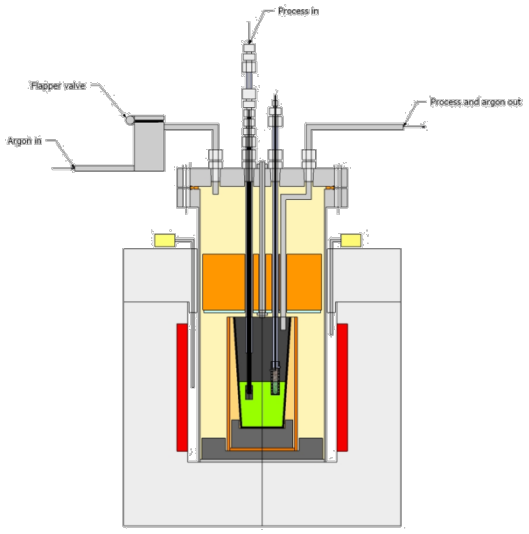

Figure 1. Reactor Design for Electrochemical Fluorination

Electrochemical modeling of the electrode reactions for the electrochemical fluorination reactions and the oxide reduction reactions was highly successful. A complete analysis of the electrochemical potentials was performed that showed that UF_6 would be the first gaseous fission

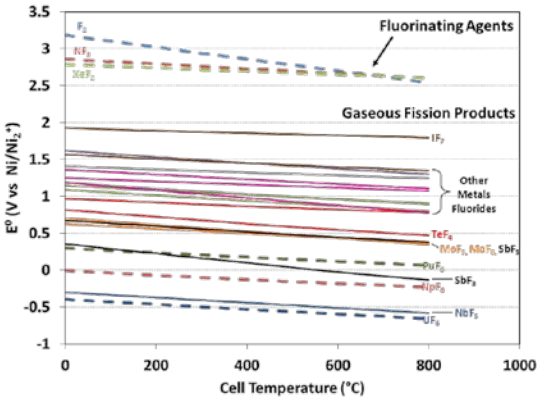

Figure 2. Equilibrium potentials for gaseous fluoride fission products.

product to be evolved from metallic UNF and would therefore facilitate separation from other UNF components. Figure 2 shows the equilibrium potentials for the gaseous products and common fluorinating agents. The results in Figure 2 show that fluorination of U to UF_6 has the lowest equilibrium potential of any electrochemical potential that produces a gaseous fission product. All of the fluorinating agents also have very high equilibrium potentials that indicate that can easily be reduced electrochemically. The kinetics of the anode and cathode reactions should not be a significant problem even when trying to selectively oxidize UNF components given the >300-mV gap between gaseous fission products near UF_6 and the high reduction potential for fluorinating agents. This shows that a galvanic cell to separate UF_6 is very feasible. The effect of activity coefficients for UNF components in the molten salt on electrochemical equilibrium potentials was determined to be negligible.

The electrochemical potentials for all reactions for molten salt constituents and UNF constituents with low equilibrium potentials such as lathanides, alkali metals, and alkali earth metals were calculated and showed that a mixture of LiF-CaF_2 may be required to separate the lanthanides by electroplating. The NaF and KF components of UNF could be reduced before the lanthanides before the lanthides. The analysis of electrochemical potentials for the oxide reduction also showed that LiF-CaF_2 would be an effective electrolyte allowing recovery of all UNF components.

A custom electrochemical reactor and electrodes have been fabricated for electrochemical fluorination (Figure 3). A system for reactor operation is nearing completion and will be used to prove the feasibility of the reactions in early FY13. The system is capable of operating the reactor with variable gas composition and pressure, while allowing recovery of the UF_6 product.

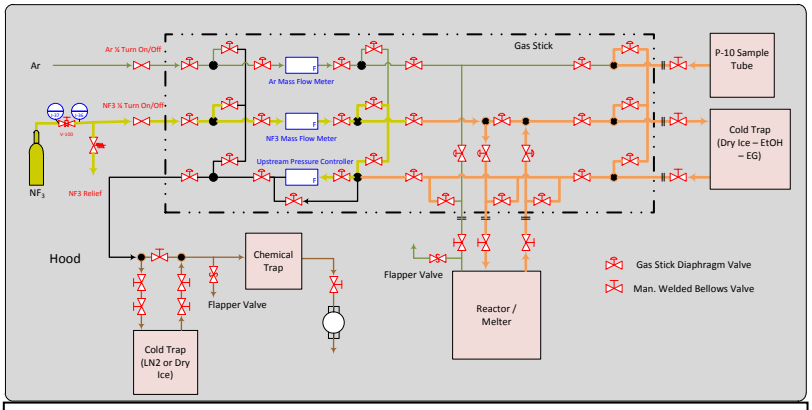

Figure 3. Reactor system for electrochemical fluorination.

The project has provided promising results for the feasibility of electrochemical fluorination and the development of a processing scheme that can start with oxide UNF. The project has also led to the submission of patent applications and full ARPA-E proposal invitations in addition to providing fundamental analysis of the process and constructing a system for proof of concept experiments. DOE and international groups working on pyroprocessing concepts have been engaged to include novel concepts from this project in roadmaps for UNF reprocessing. This included developing relationships with the University of Wisconsin and attending an international pyroprocessing conference at Argonne National Lab. The work on this project and

equipment from the project provided a foundation for SRNL to get a $3.8 million SunShot proposal on high temperature corrosion in molten salt heat transfer fluids. NEUP and FCRD proposals have also been developed relating to these concepts.

Unveiling micro-to-nano fluidics physico-chemical phenomena for advance separation and ultra-sensitive detection of nuclear species

Poh-Sang Lam, Michael G. Bronikowski, and Adrián E. Méndez-Torres

The state-of-the-art technologies based on fluidics with the characteristics of electrokinetics and electrophoresis are used to develop advanced separation processes for highly radioactive actinides and isotopes, ultra-sensitive sensors capable of detecting cementitious barrier materials degradation ion species and radionuclides migration in groundwater, as well as chemical and biological warfare agents. This work will provide cross-cutting solutions in multiple thrust areas such as fate and transport of radionuclides and chemical processing. There are two main research areas: 1) advance separation and speciation of special nuclear materials with microfluidics; and 2) nanofluidics physics and chemistry for highly selective sensing and speciation of radionuclides. Ultimately, micro/nanofluidics will be integrated in a Lab-on-a-Chip (LOC) that allows the capabilities for separation and detection up to million-folds. This project integrates SRNL expertise on fluidics, nuclear-physics, separation, concrete, modeling, and nanofabrication.

The technical objective of this proposal is to investigate and explore the underlying science and physics of microfluidics with the aim to establish SRNL in-house fluidics capabilities by adopting a "lab on a chip" (LOC) approach with multifunctional and crosscutting applications in nuclear material separation technologies and in developing trace detection sensor systems for toxic chemicals and radionuclides. For highly radioactive separations, the small size decreases ALARA concerns and permits much smaller footprints. The laminar flow in the microchannels of these chips maximizes the efficiency in molecular diffusion in an aqueous-organic liquid extraction and separation. The small sample size in microfluidics also results in fast mixing and equilibration, reduced reagent consumption, and better temperature control, facilitate the use of less stable solvents, reductants, and complexants. In sensor development with micro- and Nano fluidics, the electric double layer effects enable higher ion preconcentration which is essential for ultra-sensitive devices. This type of sensors has a potential for multiplex assay and detection for multiple analytes in parallel operation, and can be customized for measuring many targeted analytes, such as toxic chemicals and radionuclides (e.g., chloride, sulfate, Magnesium ions, nitrate, tritium, C-14, Ni-59, and Tc-99, Pu, U), proteins and DNA at various sampling station.

Two Lab-in-a-Chip Microstations are used for this project. One Microstation will eventually be deployed to the SRNL limited area for nuclear material separation. These two Microstations allow simultaneously work on separation science and on sensor development with different chips tailored for each application. A numerical modeling capability is established for benchmarking experimental results, upon which the numerical experimentation can be performed for down-selecting chip specifications or for micro/nano-channel design/fabrication. In addition, the work fully utilize the SRNL existing facilities, such as NMR, Dual Laser 3-D Micro Raman, 2-D IR, and Micro IR with environmental cell, SEM with Energy Dispersive Spectroscopy, XRD, and Mass Spectrometer.. The project team will 1) identify equipment and computation/modeling needs to establish the SRNL Fluidics Laboratory; 2) procure and install the equipment in the laboratory; 3) conduct functional testing of equipment on cold surrogates; 4) Conduct theoretical modeling for the design of micro/nano-channels to achieve high pre-concentration for ultra-

sensitive trace detection and monitoring, and for improving the LOC performance in nuclear material separation, 5) explore micro/nano-fabrication technologies for manufacturing customized LOC, 6) initiate Pu/U analogous studies using surrogates, 7) initiate the development of small scale prototype for a deployable system; and 8) seek external funding for on-going development. The work will lead to the roadmap for operation with radioactive (actinide) solutions and hazardous or biological species, and position SRNL for seeking external funding for further development in fluidics applications.

A Dolomite workstation has been installed in SRNL to conduct task on nuclear material separation. The preliminary system testing is in progress. The system has shown the capability of separating two materials with two distinct densities in the form of bubbles. Figure 1 shows a sequence of air droplets being made in a 190 micron Dolomite T-chip during initial testing of the equipment after a flow resister was placed in the air line.

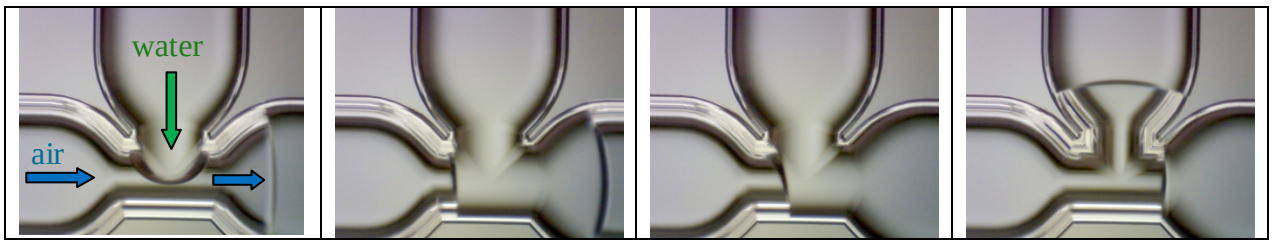

Fig. 1 Sequence of air bubbles being formed in microfluidics channel of Dolomite System.

The LabSmith workstation was set up in HTRL for sensor developing. Current effort is focused on visualization and quantification of ion concentration in fluid using dye as a surrogate. The system can be seen in Figure 2 with fluorescent image of a microchannel. The microchannel can be used with SRNL/MS&T equipment, 3D Confocal Micro Raman Spectroscope to reveal detailed concentration distribution of a chemical species in a subsurface microchannel.

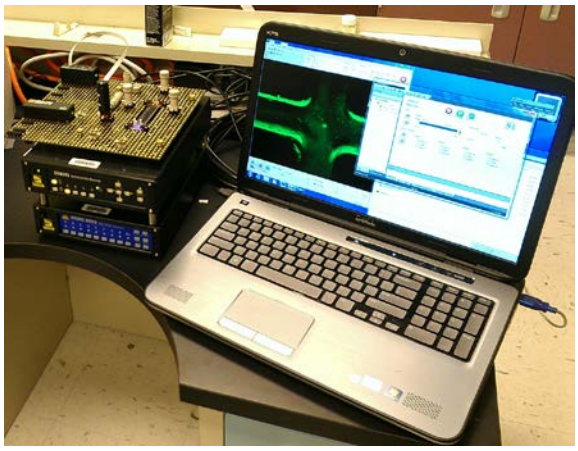
Fig. 2 LabSmith System and fluorescence microscope showing dye passing through a microchannel.

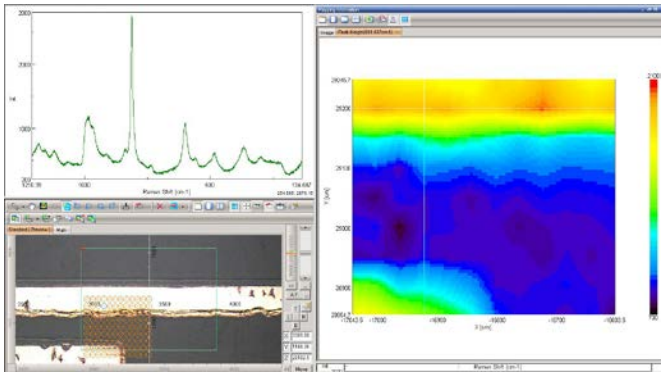
Fig. 3 LabSmith chip with 3D Confocal Micro Raman spectroscopy showing concentration intensity of the materials.

Preliminary results show that organic-aqueous separation is achievable with the Dolomite System, and ion concentration can be detected with the LabSmith workstation. The Raman-

fluidics result indicates the potential for developing high fidelity optofluidics devices for the identification of radioactive species in aqueous media. Utilizing spectroscopy techniques also allows the development of nanofluidics scintillation systems for the detection of tritium and other radioactive species.

Long-term, In-situ Monitoring of Subsurface Contaminant Stability

C. E. Turick[1], C. E. Milliken[1], H. Colon-Mercado[1], S. Greenway[2], E. Atekwana[3], and G. Abdel Aal[3]: ***[1]SRNL; [2] Greenway Energy; [3]Oklahoma State University***

We are designing inexpensive electrochemical methods to monitor the subsurface in real time, on a regular basis, in order to detect geochemical and biogeochemical changes caused by either intentional perturbations such as bioremediation or unintentional changes related to breached waste containment facilities or monitored natural attenuation. These methods are being designed for use with conventional techniques for more precise subsurface assessments. This is being accomplished through electrochemical techniques that evaluate impedance parameters related to biogeochemical changes in sediments. The inherent complexity of impedance provides a data-rich analytical platform capable of delivering specific information regarding numerous multifaceted parameters. These techniques will be used as a means to monitor progress in bioremediation activities in real-time or as a sentinel technology to serve as an "early warning system" for environmental perturbations, especially related to monitored natural attenuation or stored waste and can be run in conjunction with conventional tests for confirmation of results.

The technology we are developing will provide us with real time information about where and when to focus conventional subsurface sampling activities. Monitoring the subsurface in regard to bioremediation activities or unexpected changes related to waste containment or monitored natural attenuation is essential but time consuming and labor intensive. For example, evidence of microbial activity and subsequent geochemical alterations include: increases in cell numbers; carbon source conversion; changes in mineralogy; and soluble metal content in the subsurface. With conventional strategies, sampling activities are often minimized due to costs and could miss important data. The cost effective technology we are developing has the capability to provide abundant real-time data regarding biogeochemical changes to the subsurface without the cost of conventional sampling. These techniques will be used to monitor progress in bioremediation activities or as a sentinel technology to identify when environmental perturbations occur, especially related to monitored natural attenuation and waste containment.

Our technology is being designed to be imbedded into subsurface probes and provide electrochemical data pertaining to the subsurface without the need to pull samples. This will allow for a greater monitoring frequency that is useful in detecting unforeseen subsurface changes over time. This approach will also be useful in directing sampling activities to specific sites of interest, based on electrochemical monitoring and is designed to be run in conjunction with conventional tests as needed for confirmation of results.

This approach incorporates electrochemical techniques that evaluate impedance parameters related to biogeochemical changes in sediments. The change in properties of an electrical signal at a specific frequency passing through environmental media furnishes impedance data. This inherent complexity provides a data-rich analytical platform capable of delivering specific information regarding numerous multifaceted parameters. We are using this approach to determine changes in fluid composition, mineral composition, bacterial density and growth status, all factors that relate to environmental monitoring of the subsurface. Figure 1 below provides an example of how this approach is useful in monitoring subsurface biogeochemistry.

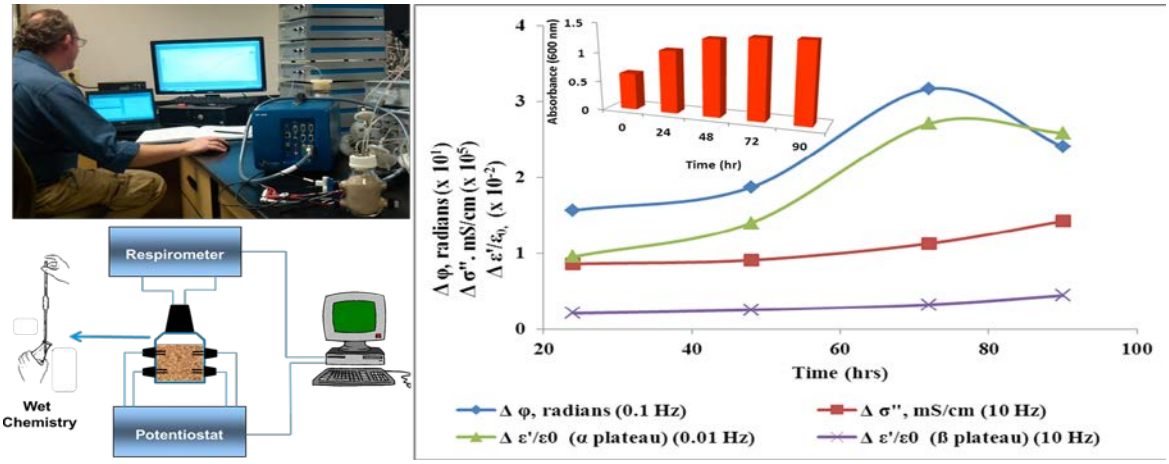

Figure 1. Correlation of microbial activity to impedance parameters. Schematic of experimental set up (bottom left) and laboratory arrangement (top left). The graph shows growth of the Fe(III) reducing bacteria *Shewanella oneidensis* MR-1 (inset) correlated to changes in: phase shift (φ, radians), indicative of biogeochemical change; conductive energy storage / polarization (σ"), correlated to increased cell number; relative permittivity ($\varepsilon'/\varepsilon_0$) (capacitance) which measures cellular activity at 0.01 Hz and cell membrane thickness at 10 Hz.

To date we have focused on impedance studies regarding: phase shift (φ), indicative to geochemical change; conductive energy storage/polarization (σ") related to cell density; relative permittivity ($\varepsilon'/\varepsilon_0$) (capacitance) measures cell membrane charge at 0.01 Hz and cell membrane thickness at 10 Hz.; as well as parameters useful in determining changes in fluid properties due to microbial growth, such as total impedance, Nyquist plots (in-phase vs. out-of-phase impedance), and changes in fluid conductivity. Our results correlate well with microbial activity and geochemical changes associated with it. In addition, we have also shown that these techniques are applicable to the vadose and capillary fringe zones along with the saturated zone. We are currently evaluating electrochemical and biological changes during active Fe(III) and SO_4 reduction. These reactions are very common in the subsurface and play significant roles in contaminant fate. Combining our impedance studies with other electrochemical techniques such as cyclic voltammetry, stripping voltammetry and chronoamperometry is providing a greater dimension to our approach and allows us to gain a better understanding of subsurface activities through these versatile techniques.

We are also comparing two impedance techniques, spectral induced polarization (SIP) developed by our university collaborators and electrochemical impedance spectrometry (EIS). SIP has been demonstrated to provide useful field information regarding microbial activity and geochemical change associated with bioremediation. EIS is a useful technique to study microbial activity and electrochemical changes associated with microbial activity. This design also allows us to exploit the versatility of our electrode configuration to incorporate other electrochemical techniques as needed.

Our approach of incorporating electrochemical techniques, especially impedance spectroscopy has enormous potential to provide valuable real-time information about changes in subsurface microbial activity and contaminant behavior in-situ. The installation of subsurface probes to monitor electrochemical parameters is expected to provide valuable and abundant information regarding biogeochemical conditions required for successful bioremediation, monitored natural attenuation and long term subsurface waste containment.

Spectroscopic Techniques for the Characterization of Particulates from Proliferation Activities

Eliel Villa-Aleman, Glenn Fugate and Robert Lascola

Abstract

Proliferation activities produce unique chemical signatures related to the manufacturing and processing of nuclear materials. Uranium (U) enrichment and the production of plutonium (Pu) are key indicators of proliferation activities. Enrichment of U via UF_6 pathway produces UO_2F_2 particulates. Extraction of Pu and metal forging also leads to the production of Pu particulates. Testing of weapon components also provide other material signatures.

Particulates from nuclear proliferation activities are of extreme importance to nonproliferation efforts of the Department of Energy (DOE) and the International Atomic Energy Agency (IAEA). Spectroscopic characterization of UO_2F_2 particulates is primarily conducted with spontaneous Raman Scattering. Raman scattering is very weak and the signal is often overwhelmed with fluorescence from the soil matrix. The detection limits of stimulated Raman scattering (SRS) and coherent anti-Stokes Raman scattering (CARS) are significantly higher. Proposed techniques will enable detection and imaging in a fraction of a time of particulates of interest.

Technical Objective/Significance

- Develop coherent spectroscopic technologies for the detection of proliferation effluents.
    - Design spectroscopic instrumentation based on Stimulated Raman Scattering (SRS) and Coherent Anti-Stokes Raman Scattering (CARS).
- Apply SRS and CARS technologies to the detection of proliferation effluents.

Research Methodology

- Identify and select the most efficient and affordable solutions for the assembly of coherent spectroscopic systems.
- Develop a continuous wave (CW) SRS laser setup for tests with uranyl compounds.
- Develop an SRS and CARS setups based on femtosecond/picosecond lasers configurations.
- Demonstrate the detection of particulates with the uranyl moiety and the enhancement expected from coherent spectroscopic techniques.
- Identify chemical structure changes due to fission and alpha tracks in polyethylene materials with SRS and/or CARS.
- Employ SRS and CARS to the analysis of particulates and materials associated with cold hydrodynamic tests.

Results/Discussion

Several designs of SRS and CARS are discussed in the literature. The different designs are tradeoffs that take into account complexity, costs, and signal to noise ratio. In order to understand the technical limitations and advantages of the experimental setups and the budgets associated with the design and development, the open literature was reviewed prior to the selection of optical and mechanical components.

During the literature review, it was found that some manufacturers of lasers were sold to competitors. The lasers were taken-off from the market or the cost doubled in price, more than expected for our budget. New experimental designs for the SRS and CARS were made to incorporate a picosecond refurbished laser equipment to accomplish the final goal. It was decided to investigate two variants of SRS and potentially two variants of CARS. One of the variant of the SRS involved continuous wave (CW) laser and the other involved the synchronization of a femtosecond and a picosecond laser. The two CARS setups include a similar synchronized femto/picosecond lasers, and a multiplex broadband setup. These experimental setups are also built in the transmissive or epi (reflection) configurations. The choices affect the design and component selection for the system. Utilities requirements such as power and cooling were identified to ensure the operation of the system during the installation. Laser safety for the wavelengths of interest was evaluated in order to procure the required laser spectacles with the proper optical density (OD).

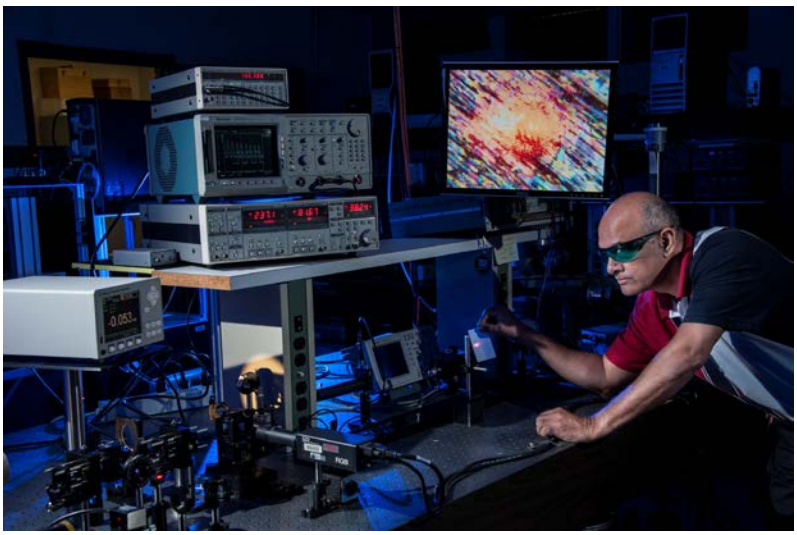

Components for the CW SRS, multiplex broadband CARS and a refurbished picosecond laser with a Synchrolock system were procured with the understanding that a pump laser for the picosecond laser would be ordered in FY14 in order to complete the synchronization with the femtosecond laser. The CW SRS system, shown on the right, was 80% completed while the optics for the broadband CARS setup was set in place and the initial alignment with a low power diode laser was completed. In order to save money in software design, LabSpec software was demonstrated to control an X-Y stage, a CCD detector and a video camera. Further tests will be required for the control of a lock-in amplifier. SRNL send the femtosecond laser to the manufacturer to test the synchronization system with the picosecond laser. Both lasers were shipped to SRNL in September.

Conclusions

Most of the components for the SRS and CARS experimental setups were procured in FY13. The high costs of the equipment procured in FY13 forced some minor changes to the design of the coherent systems. Costs cutting measurements were undertaken to redesign the scanning methodology from galvo mirrors systems for high speed laser imaging to X-Y stage point to point scanning. During FY14, the pump laser for the picosecond laser will be procured and the instrumentation will be assembled in the laboratory. The manufacturer of the laser will conduct laser alignment and final checks with the synchronization unit.

The CW setup will be completed and tested with UO_2F_2 particulates. Plastics with embedded boron will be used as surrogates for U-235 and will be irradiated in a reactor. Detection studies of fission and alpha tracks in the substrates will be completed in FY14. Detection sensitivity experiments of SRS and CARS with UO_2F_2 will be completed and samples from cold

hydrodynamic test conducted. Complete integration of X-Y stage with lock-in amplifier and LabSpec will be completed. Finally, a new approach using Quantum Coherence Control with a single laser will be considered for this project if additional funding becomes available.

Ternary carbide clad coatings and high-conductivity fuel systems for accident tolerant light water reactor fuel

Brenda L. Garcia-Diaz, Bob Sindelar, Ron Kesterson, Luke Olson, Chris Verst, Poh-Sang Lam, and Thad Adams

Air and steam oxidation of Zirconium alloy nuclear cladding during a loss of cooling accident (LOCA) rapidly evolves hydrogen, and can be extremely damaging to its mechanical integrity, potentially causing fuel and fission product release. Preventing or slowing the oxidation of the cladding by the use of coatings or other methods while maintaining a high overall efficiency has therefore become an important research priority for the nuclear industry to increase the safety envelope of the present US nuclear fleet. This project investigates methods to synthesize, optimize, and test MAX Phase coating performance characteristics and to model how the materials will improve the behavior of nuclear fuel during LOCA events. Results have identified that a sprayed coating of commercially-available MAX Phase Ti_2AlC has excellent corrosion resistance and strength during LOCA events. Further, the negative reactivity of MAX coatings is negligible or can be addressed through minor enrichment of the fuel.

During LOCA nuclear accidents such as the ones at Fukushima and Three Mile Island, nuclear fuel can be exposed to air and steam at high temperatures reaching 1200°C. The zirconium alloy cladding readily oxidizes under these conditions through reactions with both steam and water to form ZrO_2 and H_2. Continued rapid corrosion can ultimately cause breakdown of the cladding, and potentially expose the nuclear fuel to the environment and lead to significant radioactive contamination. Coating the cladding to form a diffusion barrier to steam and oxygen which prevents oxidation of the cladding at high temperatures is of interest in stopping the copious generation of hydrogen and the catastrophic failure of the cladding. MAX phase materials such as Ti_2AlC have high thermal conductivity and high mechanical strength similar to metals while having oxidation and chemical reaction resistance similar to ceramics. These properties would minimize the impact of the coatings on efficiency during normal operation and would enhance the safety of the cladding during a LOCA event. This project is working to develop methods for coating cladding and understand the viability of the MAX coatings as a protective barrier through experimental and modeling efforts.

The MAX phase coatings in this project are synthesized by cold-spraying of MAX powder onto Zircaloy 4 (Zry 4) substrates. The cold-spraying method uses high velocity impact of MAX particles with mechanical bonding to adhere the coating to the Zry 4 surface. The oxidation resistance properties of the coatings are measured during normal operation through tests with pressurized steam near 300°C and in steam tests at 1200°C and atmospheric pressure. The mechanical and adhesion properties of the coated cladding will be measured through scratch testing, hardness testing, and wear testing. The impact of coatings on neutronics performance (reactivity of MAX-coated cladded fuel) will be measured using Monte Carlo simulations. Modeling of the mechanical properties of the coatings will be performed using finite element modeling. Modeling and coating synthesis will both be used to identify optimal coating properties including the thickness, MAX composition, and synthesis conditions. Characterization of how MAX phase additives to the nuclear fuel can improve thermal conductivity and increase both efficiency during normal operation and safe dissipation of heat during LOCA events. Where applicable, results from SRNL projects and other research groups, such as an NEUP with Drexel University, were used to guide the research on this project.

Mechanical and neutronics modeling of MAX phase materials under normal operations and LOCA conditions have been performed to identify the best potential candidate materials for MAX phase coatings and optimal thickness for the coatings. The mechanical modeling using Finite Element Analysis (FEA) clearly showed that Ti_2AlC had improved high temperature strength compared to Ti_3AlC_2 and is a viable coating material. The Ti_2AlC and Ti_3AlC_2 were chosen as the preliminary candidates for MAX phase coating on cladding because they have been shown to have excellent high temperature properties and are commercially available. Neutronics modeling showed that the reactivity impact of coating thicknesses of 100 microns would be significant enough to reduce the power efficiency of the fuel core; further, increased dimensions to slide the fuel into the grid plates would be needed to accommodate fuel with coatings of this thickness and above. Figure 1 shows the neutronics modeling results and analysis. The modeling showed that while thinner coating always had less impact (higher reactivity or K-eff) than thicker coatings, coating thicknesses around 25 microns and up to 50 microns could have a relatively minimal impact on reactivity while simplifying cold-spray procedures which are not traditionally used for thin coatings. A subcontract has been put in place with the University of Wisconsin for coating Zry-4 substrates with Ti_2AlC with thicknesses on the order of 50 microns based on these results. In addition to only cold-spraying the coatings, post-treatment methods of the coatings such as laser annealing are being tried to improve adhesion of the coating to the substrate and reduce coating porosity based on some images that were published by other groups that have performed research on cold spray MAX coatings for other applications.

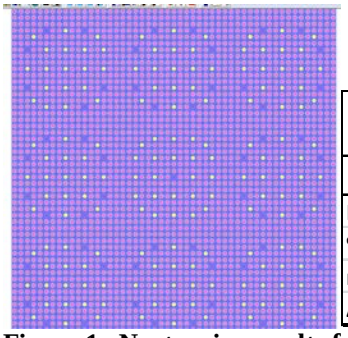

Critical Case , K =1					
	Zirlo - **Uncoated**	Ti_2AlC - **5µm**	Ti_2AlC - **10µm**	Ti_2AlC - **25µm**	Ti_2AlC - **100µm**
K-eff	1.0004	0.9994	0.9942	0.994	0.9724
% change in k	N/A	-0.100%	-0.620%	-0.640%	-2.799%
reactivity, ρ	0.0004	-0.0006	-0.0058	-0.0060	-0.0284
Δρ	N/A	-0.0010	-0.0062	-0.0064	-0.0288

Figure 1. Neutronics results for Ti_2AlC Coatings on Zirconium Alloy Cladding

Scratch testing and steam testing capabilities have been developed and demonstrated at SRNL. A Nanovea mechanical tester has been set up and commissioned in the SRNL Energy Materials Research Laboratory (EMRL) facilities for performing scratch testing of samples as well as hardness and wear testing. Reactors and furnaces for being able to perform pressurized steam testing up to 315°C have been set-up along with performing safety analysis of operation. Reactors and a boiler for performing atmospheric pressure tests up to 1200°C to simulate LOCA conditions has also been set-up and commissioned for testing.

The modeling, synthesis, and testing of MAX coatings on Zry 4 has the opportunity to improve the safety of nuclear fuel in the event of beyond-design-basis LOCAs, and also afford reduced corrosion during normal operation and design-basis LOCAs. A systematic plan to define the MAX coatings parameters along with the synthesis and testing protocols has been put in place and the synthesis of coatings along with verification of testing protocols is currently underway. The experimental plan is focusing on Ti_2AlC coatings with a thickness of 30-60 microns that

were identified by mechanical and neutronics modeling as having the best opportunity for success with materials that are commercially available.

Structural integrity of dual-purpose canisters for used nuclear fuel under extended storage and transportation

P.S. Korinko, P.S. Lam, R.L. Kesterson, A.J. Duncan, E.A. Clark, T.M. Adams

Two aspects of the structural integrity of dual-purpose (extended storage and transportation) canisters for used nuclear fuel are being studied. First, fracture assessment methodologies are applied to the canisters under both extended storage and transportation conditions. Fracture mechanics based flaw stability acceptance criteria will be established to assure pits and cracks caused by marine and industry deposited salt will not cause canister failure. The second aspect is directly applicable to the fuel being stored and transported inside the canister. Two tests of the ductility of hydrided fuel cladding are being compared and evaluated to ensure they demonstrate sufficient ductility exists for normal and off-normal loads during transportation and storage of used nuclear fuel.

Two important issues facing the nuclear industry in the continued extended storage of sealed stainless steel canisters in Dry Cask Storage Systems at Independent Spent Fuel Storage Installations are i) their vulnerability to pitting and cracking of the canister (caused by marine salt and industry deposit contaminants) and ii) the reduction of ductility of zirconium alloy fuel cladding caused by hydride formation during reactor operation and storage. First, the canister is the safety-credited containment boundary of the storage and transportation system, and it must contain the used fuel during normal storage and transportation and during accidents. Second, during reactor operation circumferentially oriented hydrides form in zirconium alloy fuel cladding (from hydrogen produced by surface corrosion), and these nascent rim hydrides can reduce the ductility of the cladding, however, they are not as potentially detrimental as radial hydrides that may form during drying and dry fuel cask storage. The cladding ductility is required to be sufficient during used fuel storage and transportation so that the used fuel cladding retains its integrity- it must contain fuel particles and fission products- during normal and off-normal loads (accidents) while in storage and during transport.

This program is addressing both of these issues. First, fracture mechanics assessments for postulated flaws in the welded regions of the stainless steel dual-purpose canister are being conducted. Acceptance criteria for flaw disposition will be established if flaws and defects are found by canister in-service inspection programs. Second, the ductile-to-brittle transition temperature of radially hydrided zirconium alloy tubing will be measured using two tests: the currently used “ring compression test” will be compared with a three-point bend test. The three point bend test is more realistic because i) the applied loads on used fuel cladding in storage containers are likely to be “three point bend” type loading and ii) there is effectively no clearance between the pellet OD and clad ID to accommodate the deformations necessary for ring test type failure strains.

The procedure prescribed in the American Petroleum Institute API 579 Fitness-for-Service was found to be a plausible approach when the realistic material properties of the canister (base and weld metals) are obtained from literature and the canister stress analyses were carried out separately by various organizations (e.g., from NUREG-1864, U. S. NRC, 2007). The failure assessment diagram (FAD) based approach will be adopted to develop the flaw disposition methodology. Experimental apparatus to dissolve hydrogen into zirconium alloy tubing representative of nuclear fuel cladding has been fabricated and successfully tested, and another

apparatus to form “radially oriented” zirconium hydride in the tube wall has also been fabricated and successfully tested. This apparatus applies sufficient circumferential stress so that radially oriented hydrides form in addition to the initially formed circumferential hydrides. Techniques of surface polishing for microscopy of zirconium alloys have been developed, and both circumferentially- and radially-oriented hydrides have been observed to form in samples, as determined by electron microscopy of sample tube sections. It is well known that used nuclear fuel is subject to radially oriented hydrides during dry out annealing and that these hydrides affect the ductility of the cladding. The ductility of used nuclear fuel cladding as measured by the ductile-to-brittle transition temperature is critical in modeling and determining safe temperatures for transport, handling and storage. Also, as a confirmation of the testing procedure, initial ring compression tests of samples at SRNL duplicate results found in the literature. SRNL is now able to reliably create samples having sufficient hydrogen and the hydride microstructure (radial orientation) of interest in assessing the performance of zirconium alloy fuel cladding.

Work planned for FY 14 for the structural integrity of the canisters is to extract necessary mechanical and fracture properties as well as the critical stresses from the published documents and input the information to the API 579 procedure for flaw evaluation and to develop the acceptance criteria for in-service inspection. Work planned for FY 14 for the zirconium alloy radial hydride ductility includes developing the pre-hydrided clad three-point bend test, creating a set of zirconium alloy samples with realistic amounts of radial hydride and characterizing the hydrogen content and hydride morphology. Both the ring compression and three-point-bend tests will be used to test sample ductility as a function of temperature to the “ductile-to-brittle transition temperature” as a function of test method and hydride morphology/content. Later, the effect of cooling rate on radial hydride formation will be investigated via the circumferential stressing procedure. Previous work by other laboratories have used a rapid cooling rate compared to that expected for actual fuel cooling after the dry-out anneal, and the slower rates are expected to provide more representative and realistic hydride formation characteristics.

Development of Glass and Glass Ceramic Proppants from Gas Shale Well Drill Cuttings

F.C. Johnson, K.M. Fox, J.C. Marra and J.R. Hellmann

Drilling of natural gas wells creates large quantities of drill cuttings that contain Technology Enhanced Naturally Occurring Radioactive Materials (TENORMs), along with significant quantities of mineral oil. These hazardous components require that cuttings be disposed of in engineered landfills at significant expense. Converting these materials into proppants for use in hydrofracturing the geological strata from whence they came offers a unique opportunity to sequester these materials in an environmentally benign manner. Using SRNL flame spheroidization technology, glass spheres with average diameters of 75-100 µm were produced from vitrified drill cutting feed sized to less than 90 µm. Additives increase the average diameters of the resulting spheres to approximately 125 µm; however, considerable surface inhomogeneities are present, which would be detrimental to the mechanical properties of the proppants. Direct fusion of drill cuttings is infeasible with the current system. Design modifications to the existing flame former system would be required to achieve the desired proppant diameter of 0.5-2.0 mm. A longer residence time in the heated zone is necessary for fusion of either actual drill cuttings or vitrified drill cuttings. It is also possible that a higher temperature gas mixture would also be needed to optimize the melt viscosity for spheroidization.

The objective of this work was to develop a method of converting drill cuttings from gas shale wells, which contain TENORMs, into high strength proppants via flame spheroidization and devitrification processing. These hazardous components require that cuttings be disposed of in engineered landfills at significant expense (nominally 1000 tons/well at $60/ton disposal costs). Previous research by The Pennsylvania State University (PSU) has shown that proppants (ceramic particles used for retaining permeable paths in hydrofractured gas and oil wells) can be manufactured from residual mine tailings, similar in composition to the drill cuttings, via pelletization and melt fusion/devitrification processing. These proppants exhibit excellent strength, fracture toughness, crush resistance and long term conductivity, all of which are important prerequisites for acceptance by the well completion industry. Extension of this technology to drill cuttings containing TENORMs is timely and of distinct importance to the unconventional oil and gas production industry. Recycling of drill cuttings for proppant use represents a unique application in the multi-billion dollar proppant manufacturing market.

The Pennsylvania State University provided SRNL with three size fractions of drill cuttings; as received drill cuttings (unsieved, -16/+35 mesh and -35 mesh). These drill cuttings were characterized for chemical composition via inductively coupled plasma-atomic emission spectroscopy (ICP-AES), scanning electron microscopy-electron dispersive spectroscopy (SEM-EDS), thermogravimetric analysis coupled with mass spectrometry (TGA-MS), Fourier Transform Infrared Spectroscopy (FTIR) and crystallinity via X-ray diffraction (XRD). Two methods for proppant formation were explored using SRNL flame spheroidization technology; direct fusion of drill cuttings and spheroidization of vitrified drill cuttings. The flame former system is based on a Hauck Manufacturing propane/air inspirator burner. Flowing air pneumatically transfers feed to the burner where the propane is introduced. Air, propane gas, and feed are passed through a flame where particles soften and spheroidize. Various size fractions of feed stock were utilized throughout the process. Based on the high silica content of the vitrified drill cuttings, some experimentation with various additives was also conducted in order to reduce

the melt viscosity and ease of spheroidization. All particles were examined with optical microscopy and/or SEM-EDS post flame forming. Due to the large target diameter of proppants (0.5-2.0 mm), higher temperatures and longer residence times in the heated zone are required to spheroidize particles. It is likely that spheroidization from a melt as opposed to solid particles could be more effective than the flame former. Thus, drain tube configurations for the formation of discrete droplets were also investigated to be used with an induction melter. In order to more safely and efficiently evaluate the parameters, a room temperature mock-up was used with high viscosity oils characteristic of molten drill cuttings.

Qualitatively, the major phase in the drill cuttings is quartz, with minor phases consisting of barite, chlorite-serpentine, muscovite, calcite, and enstatite. Post vitrification, the material is completely amorphous with an average composition of $16Al_2O_3$-4CaO-$5.6Fe_2O_3$-$64.4SiO_2$-10 Others (wt%). A total mass loss of approximately 17% is measured after heating to 1000°C. MS and FTIR analysis identified the release of various carbon and sulfur species during heating. Direct flame spheroidization of the drill cuttings was attempted first, as this method is the simplest and least expensive for a production scale operation. Drill cuttings sized to -16/+35 mesh were relatively unaffected by the flame, although significant agglomeration was observed with the -35 mesh particles. The next fabrication method added a melting step to vitrify the drill cuttings and a grinding step to produce the appropriate size fraction for flame spheroidization. Multiple size fractions were used to determine how fine the particles needed to be for spheroidization using the flame former in its current configuration. Softening of the particles becomes more apparent as the particle size of the feed material is reduced, with spheroids becoming evident in the material screened to -170/+270 mesh. The material screened to -270 mesh resulted in the production of well-formed spheres. While these spheres are likely too small for use as proppants, they prove the concept of converting drill cuttings into spherical particles.

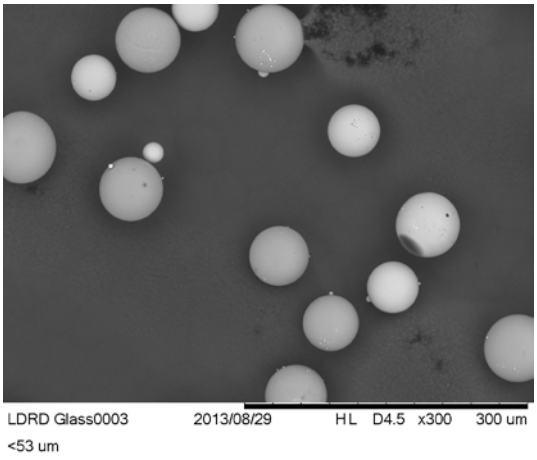

Flame spheroidization of *vitrified* drill cuttings is possible; however, size limitations exist. Success of the process is dependent on the size of the feedstock. Glass spheres with average diameters of 75-100 µm were produced using feed sized to less than 90 µm and the highest percentage of spheres (average diameters of 50-90 µm) was obtained using feed sized to less than 53 µm. In general, the spheres produced using the smaller feed size (< 53 µm) contained surface inhomogeneities, which would be detrimental to mechanical properties. The use of additives mixed with the drill cuttings yields spheres with average diameters of approximately 125 µm, but significant surface inhomogeneities are present. Direct fusion of drill cuttings is infeasible with the current SRNL technology. In either of these methods, longer residence times in the heated zone would be necessary for the fusion and spheroidization of the high silica-based drill cuttings in order to achieve the desired proppant diameter (0.5-2.0 mm). Design modifications to the existing flame former system would be required to achieve a longer residence time. It is also possible that a higher temperature gas mixture would also be needed to optimize the melt viscosity for spheroidization. Room temperature drain tube testing indicates that it is possible to produce discrete drops of oil at viscosities similar to those expected for the proppants at elevated temperatures (1300-1500°C). The immediate challenge would be to refine

the process to increase flow rate, which may be feasible with an array of drain tubes. Another possibility would be to initiate drops through the use of an air purge.

Identifying Optimal Applications for Low-cost, Highly Effective Sorbents for Cs, I, and Tc

Daniel I. Kaplan, Anna S. Knox, P. Crapse, Dien Li, and David P. Diprete

The objectives of this study were to conduct a series of laboratory studies to evaluate low-cost and highly effective sorbents for $^{99}TcO_4^-$, $^{129}I^-$ and $^{137}Cs^+$ removal from contaminated aqueous and sediment systems. More than 230 batch sorption measurements were made. Two organoclays, OCB and OCM, demonstrated not only large sorption capacities for TcO_4^- ($K_d > 10^5$ mL/g), I^- ($K_d \geq 10^4$ mL/g), and Cs^+ ($K_d > 10^3$ mL/g), but also bound the radionuclides in a largely irreversible manner. Activated-carbon GAC 830 was effective at sorbing TcO_4^- ($K_d > 10^5$ mL/g) and I^- ($K_d = 10^3$ mL/g), while a surfactant-modified chabazite was effective at sorbing TcO_4^- ($K_d > 10^4$ mL/g) and Cs^+ ($K_d > 10^3$ mL/g). In addition, modified zeolite-Y was effective for TcO_4^- removal ($K_d > 10^5$ mL/g), AgS was effective for iodine ($K_d = 10^4$ mL/g). Several sorbents were identified to be affective for Cs (K_d values $> 10^3$ mL/g). A proof-of-concept demonstration using ^{99}Tc-contaminated sediment and select sorbents was successful. A patent and manuscript describing these results were submitted.

The objectives of this study were to 1) evaluate low-cost sorbents for the uptake of $^{99}TcO_4^-$, $^{129}I^-$, and $^{137}Cs^+$; 2) quantify the tendency for Tc, I, and Cs to desorb from sorbents under extreme pH conditions, and 3) evaluate the benefit of mixing sorbents on radionuclide removal from the aqueous phase, and 4) conduct a proof-of-concept with a SRS, ^{99}Tc-contaminated sediment. A unique attribute of this work is that it targeted not only highly effective, but also low-cost sorbents. This project is applicable to all three LDRD Focus Areas because the technology can be used for the *Nuclear Environmental Stewardship Focus Area* (Cs, Tc, and I environmental remediation, especially at SRS and Hanford Site), *Nuclear Fuel-Cycle Focus Area* (especially Tc separation from waste streams under oxidizing conditions), and *Non-Proliferation Focus Area* (Cs – weapons of mass effect; WME).

A series of batch experiments were conducted in which the sorbents were added to individual centrifuge tubes containing groundwater amended and $^{99}TcO_4^-$, $^{129}I^-$, or $^{137}Cs^+$. There were four studies: 1) survey of 25 sorbents to quantify distribution coefficients (K_d values; $rad_{surface}/rad_{aq}$); 2) desorption experiment of radionuclides from sorbents at extreme pH levels: pH-3 and -10; 3) evaluation of synergistic benefit of mixing sorbents, and 4) a proof-of-concept experiment in which 0, 0.5, or 5 wt-% of sorbents were added to an SRS sediment contaminated with ^{99}Tc. Together, >230 separate adsorption and desorption measurements were conducted.

Table 1 shows the (ad)sorption K_d values for several of the sorbents evaluated. Some key conclusions include:

- **Very effective for $^{99}TcO_4^-$:** Activated Carbon (GAC830), Organoclay-OCB & -OCM, Modified Chabazite, Modified zeolite-Y (Table 1)
- **Very effective for $^{129}I^-$:** Activated Carbon (GAC830), Organoclay-OCB & -OCM, Argentite (Table 1)
- **Very effective for $^{137}Cs^+$:** Several minerals, but many are not much better than naturally occurring minerals (Table 1)

- **Radionuclide desorption from sorbents:** little Tc, I, or Cs were released from the sorbents when the system pH was adjusted to pH 3 or pH 10 (except for I from Organoclay OCB) (data not shown)

Table 1: ^{99}Tc, ^{129}I and ^{137}Cs K_d (mL/g) values of select sorbents in artificial groundwater (pH 5.5).

Sorbent	Tc K_d	I K_d	Cs K_d
SRS sediment	0.6-1.8	0.3-0.9	10-50
Activated carbon 824 BC	120 ± 41	12 ± 5	21 ± 13
Activated carbon GAC 830	(>1.08 ± 0.03)×10^5	>6.92 ± 0.22×10^3	192 ± 50
Apatite II	223 ± 8	N/A	N/A
Chitosan	54 ± 6	88 ± 1	134
Illite (IMt-2)	N/A	N/A	(>1.17 ± 0.39)×10^4
Organoclay OCB	(>1.17 ± 0.07)×10^5	>9.61 ± 0.63×10^3	(>2.80 ± 0.57)×10^3
Organoclay OCM	(>1.12 ± 0.01)×10^5	>2.93 ± 0.04×10^4	(>1.23 ± 0.11)×10^3
Argentite (AgS)	N/A	>2.5×10^4	N/A
Engineered Herschelite (KUR-EH)	0 ± 5	0 ± 2	>4.0×10^4
Zeofume (Engineered Herschelite fines)	0 ± 0	0 ± 2	>8.63×10^3
Surfactant-modified Chabazite	(>2.56 ± 0.11)×10^4	122 ± 13	>6.59×10^3
Modified clinoptilolite (KUR-SMZ)	247 ± 59	6 ± 7	>6.09×10^3
Modified zeolite Y	(>2.35 ± 0.01)×10^5	N/A	N/A

N/A = not available

[a] Experimental conditions included: 2-4 replicates, ambient temperature, 10 g/L sorbent in artificial groundwater, initial spike concentrations of 4.51×10^3 pCi/mL $^{99}TcO_4^-$, 451 pCi/mL $^{129}I^-$, and 22.5 pCi/mL $^{137}Cs^+$, 7-day contact time, phase separation by settling and 0.45-µm filter.

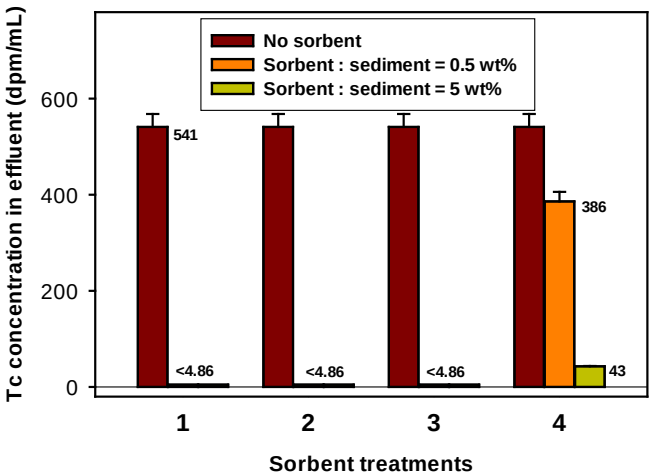

Fig. 1. Proof-of-Concept. Performance of selected sorbents for the

- **Synergistic sorption from mixed-sorbent beds:** none noted

treatment of Tc-contaminated SRS clayey sediment. Sorbent treatments: 1 = activated carbon GAC 830; 2 = organoclay OCB; 3 = organoclay OCM; 4 = surfactant modified chabazite.

- **Proof-of-Concept**: 3 out of 4 sorbents were shown to be very effective at reducing porewater ^{99}Tc concentrations from sediments contaminated with ^{99}Tc (Fig 1)

The key conclusions from this research are the following:

- **Patent Disclosure:** Kaplan, Knox, Crapse, Li, Diprete. 2013, Organo-modified clays for removal of aqueous radioactive anions. SRS-13-005. June 3, 2013. SRNS, LLC
- **Manuscript:** Li, Kaplan, Knox, Crapse, and Diprete. 2013. Removal of aqueous ^{99}Tc, ^{129}I, and ^{137}Cs from contaminated groundwater and sediments using highly effective, low-cost sorbents. *J. Hazardous Materials* (Submitted).
- **Identified several sorbents** that are low cost and highly effective
- **Proof-of-concept** was successful (Fig 1)

Novel Materials for Radionuclide Separations

K. M. L. Taylor-Pashow (SRNL), W. Lin (UNC, U. Chicago), C. W. Abney (UNC, U. Chicago)

This project aimed to prepare and evaluate novel materials for radionuclide separations for a variety of applications related to DOE missions. Target applications included treatment of high level nuclear waste, minor actinide/lanthanide separations for fuel cycle application, and remediation of contaminated seawater like that resulting from the Fukushima Daiichi nuclear disaster. A unique ligand extraction process using metal-organic framework templates was used to prepare a series of highly porous inorganic sorbent materials containing Ti and Zr. Variations of these materials showed promise in each of the applications previously mentioned. Results generated from this work lead to the filing of a provisional patent covering the new materials and the synthetic technique used.

There is a need for the separation or extraction of actinide elements in many fields relevant to the DOE mission, for example, nuclear waste processing, environmental clean-up, and development of sustainable nuclear fuel cycles. The objective of this research project was to develop new materials with high selectivity for the separation of radionuclides under a variety of conditions. Target applications included treatment of high level nuclear waste (HLW), minor actinide/lanthanide separations for fuel cycle application, and strontium removal from contaminated seawater like that resulting from the Fukushima Daiichi nuclear disaster.

Metal-organic frameworks (MOFs) are highly porous coordination polymers composed of organic bridging ligands and inorganic secondary building units (SBUs), which can be either individual metals or metal clusters. In this work, we have taken advantage of the lability of metal-ligand coordination bonds in MOFs, and used the MOFs as templates to prepare six new stable and porous inorganic materials by a novel, controlled ligand extraction process. Precise removal of the organic ligand results in the preservation of MOF SBUs which are topotactically linked by inorganic groups (such as phosphate and hydroxide) to yield highly porous and robust inorganic materials that retain the morphologies of the original MOF templates. The resulting porous and stable inorganic materials are highly effective as sorbents for decontamination of HLW, lanthanide extraction, and remediation of radioactive seawater simulating the contaminated cooling water from the Fukushima Daiichi disaster.

MOF templates MIL-125 and UiO-66, with framework formulas $Ti_8O_8(OH)_4(BDC)_6$ and $Zr_6O_4(OH)_4(BDC)_6$ (BDC = 1,4-benzenedicarboxylate), respectively, were prepared by solvothermal syntheses.[1] [2] To prepare the inorganic sorbents the MOF templates were suspended overnight in aqueous solutions of NaOH, Na_3PO_4, or H_3PO_4, followed by collection via centrifugation and multiple washes with water to yield porous oxide (MOx), oxyphosphate (MOxyPhos), and phosphate (MPhos) materials, respectively, where M = Ti or Zr. TGA measurements confirmed complete removal of the organic bridging ligands and PXRD revealed the materials were amorphous. Observation by electron microscopy revealed the inorganic materials retained the morphology of the original MOF precursor. Brunauer-Emmett-Teller (BET) analyses of the materials revealed that the porosity was preserved.

[1] Dan-Hardi, M.; Serre, C.; Frot, T.; Rozes, L.; Maurin, G.; Sanchez, C.; and Férey, G., *J. Am. Chem. Soc.*, **2009**, *131*, 10857-10859.

[2] Cavka, J. H.; Jakobsen, S.; Olsbye, U.; Guillou, N.; Lamberti, C.; Bordiga, S.; and Lillerud, K. P., *J. Am. Chem. Soc.*, **2008**, *130*, 13850-13851.

Performance of the NaOH and Na_3PO_4 treated materials for strontium and actinide separations in HLW was evaluated using a simulated waste solution representative of typical SRS HLW. Monosodium titanate (MST) and modified MST (mMST) were included in the test sets for comparison. Materials were added at equivalent Ti concentrations, while Zr materials were added at approximately one-half molar equivalent. All porous inorganic materials were found to have greatly enhanced Sr removal versus the MST control. In particular, the ZrOxyPhos had dramatically higher DFs than the MST or the other materials tested, further amplified by being added at approximately one-half molar equivalent to MST. Both ZrOxyPhos (added at a Zr concentration of 1.05 mM) and mMST (added at a Ti concentration of 2.01 mM) removed Sr to below the method detection limit prior to the 6-hour sampling time. However, the ZrOxyPhos appears to have more rapid Sr removal kinetics as seen by the increased DF after 1 hour of contact. The 1-h Sr DF values were 145 and 239 for mMST and ZrOxyPhos, respectively, at the given concentrations. The materials also showed excellent Pu removal performance, with Pu DFs similar to that obtained by MST when added at approximately half the concentration.

The second radionuclide separation application investigated was minor actinide and lanthanide separation, which is a key area of research for closing the nuclear fuel cycle. Experiments were performed to examine the affinity of the MOF-derived materials for lanthanides under acidic conditions relevant to nuclear fuel reprocessing. Experiments were performed at both pH 3 and 6 using a Ln stock solution and the oxide and phosphate materials (Ti and Zr). The materials performed better at higher pH where both the TiOx and ZrPhos showed excellent performance. The TiOx removed greater than 98.5% of all of the lanthanides in the test solution, while the ZrPhos material performed slightly better, removing greater than 99% of all lanthanides present. These two materials also showed high affinities for Am^{3+} in pH 6 solution. Separation factors of 21 and 16 were obtained with TiOx for La/Am and Nd/Am, respectively.

The third and final application investigated was removal of radioactive strontium from simulated seawater. This application is relevant to the clean-up of the Fukushima Daiichi disaster site where large amounts of contaminated seawater that was used for cooling is currently being stored and treated to reduce the radioactivity. One of the major contaminants needing removal is ^{90}Sr. Experiments were performed using the oxide, oxyphosphate, and phosphate materials in simulated seawater containing Sr. MST and SrTreat® were tested under the same conditions as a basis for comparison.

Of all of the materials tested, TiOxyPhos appears the most promising, removing greater than 70% of the Sr in seawater simulant within 1 hour. TiOx was competitive with MST and SrTreat, with each material removing approximately 50% of the Sr in solution. On a mass of metal (Ti or Zr) basis the Ti materials outperform the Zr materials in general; however, due to the difference in atomic masses, the Zr materials are present at approximately half of the molar concentration.

In conclusion, we have prepared a series of porous inorganic materials via topotactic transformations of MOF templates. This novel ligand extraction process allowed the preservation of the MOF SBUs to lead to the first well-defined porous Ti and Zr materials as well as new porous metal phosphates that are prepared from MOF templates. By varying the digest solution, we successfully tuned the compositions, surface areas, and pore sizes of the resulting materials for three different radionuclide separations. ZrOxyPhos was superior in decontaminating HLW simulant, while both ZrPhos and TiOx extracted almost all Ln from slightly acidic aqueous solution, and TiOxyPhos showed significant affinity for Sr in seawater. The rapid uptake of radionuclides in these experiments surpassed the state-of-the-art sorbents due to the high porosity and the well-defined morphologies of these novel materials

Detection of Fluoride and Uranium Exposure in Terrestrial Plants

M.C. Duff, W.W. Kuhne, N.E. Halverson, E. Caldwell, C. Milliken, K.C. Hardin, A. Washington and C. Stafford.

Fluoride ion (F^-) and uranium (U) can be toxic to terrestrial plants and their individual or combined effects are readily observed at high exposure concentrations. Low exposure concentrations of these contaminants can be detected through analytical measurements of tissues but the potential exists for even lower exposure levels to be detected in plants through omics-based approaches, which do not rely on the direct measurement of the contaminant. Lab studies were performed with plants that were exposed aerially to known amounts of $U(VI)O_2^{2+}$ and F- solutions at known pH values. The plant shoot tissues produced omics responses that were time-, concentration- and pH-dependent. The responses were also unique in terms of the gene regulation response—in magnitude and total number. This report briefly summarizes the results. Due to its required brevity, this report does not include a discussion of plant omics response mechanisms.

Several research studies have been performed on the phytotoxic effects of F and U. These studies have included gross physical observations as well as biomolecular measurements of metabolites and enzymatic reactions. To our knowledge, omics-based measurements have not been used to evaluate the effects of these elements at the larger scale gene and protein regulation level. This study aims to detect omics responses of plant shoot tissue to known levels of topically-applied $U(VI)O_2^{2+}$ and F^- ions. The findings have applications within agriculture (in terms of F-based fumigant application and insect predation) and environmental chemistry (such as acid rain and air pollution monitoring), as well as human health.

This research utilizes state-of-the-art techniques that are currently used for cancer research as well as other medical and agricultural applications. The work is accomplished by exposing plant shoot portions via spraying with 1 mL solutions of dissolved U, F, and U+F and allowing the plants to grow for 24 or 196 h post exposure. Equimolar solutions of NaF and LiF were tested individually to determine possible cation-specific effects. Two pH values were selected to study the influence of pH on plant response with dissolved U and F. The plant tissues were allowed to dry after spraying for 2 h and then they were placed in their growth chamber until harvest. The plant shoot tissues were harvested after 24 and 196 h of spraying. The tissues were preserved at low temperature until extraction for their RNA and protein at SRNL. The extracts were then provided to a university with the collaborative expertise to perform high throughput transcriptome (TRANS) and proteomic (PROT) analysis. After analysis, the data were run by SRNL through a series of statistical calculations to observe changes in response relative to that of a control (using a Log 2-based fold-change method). Those data that meet a set *t*-test value of significance are then determined and the biomolecular role of those genes (from the TRANS) and proteins (from the PROT).

Visual observations showed that the plants that were allowed to grow for 24 h after spraying exhibited minimal shoot damage relative to those that were allowed to grow for 196 h. Those plants that were sprayed with pH 3 solutions were the most adversely affected. Photographs reveal that the beading up of the sprayed solution often led to mottling on the tissues after 196 h. The mottling was typically yellow, which is indicative of leaf chlorosis (loss of chlorophyll).

The following can be concluded from the TRANS results for plant shoot tissues (based on the data having a *t*-test P-value $\leq$0.05):

- Gene responses were larger in magnitude (based on a Log 2 fold-change of the treatment relative to a control) when the plants were sprayed with 100 μM U than with 10 μM U.
- Plants exposed to 10 μM U had twice as many genes that were significantly affected than plants that were exposed to 100 μM U for equal amounts of time.
- Gene up-regulation responses in plants after 24 h from spraying were larger in magnitude than that of plants after 196 h from spraying under the same exposure conditions.
- Plants that were sprayed and allowed to stand for 24 h had fewer numbers of impacted genes than plants that were allowed to stand for 196 h after spraying. This suggests that it takes time to provoke the expression of some genes but the overall amount of gene expression of the early response genes generally decreases with time. This suggests the plants can recover but there is some "memory" of the plant exposure in the gene expression 1 week after exposure.
- After 196 h, plants that received spraying with a pH 3, 100 μM U(VI) nitrate + 600 μM NaF solution had a very large number of genes that responded relative to the plants that were sprayed with a pH 6, 100 μM U(VI) nitrate + 600 μM NaF solution (~4,500 genes at pH 3 vs. ~320 genes at pH 6). This suggests that acidity greatly influences plant response to U and NaF.
- Plants responded more in terms of down- or up-regulation level when sprayed with 600 μM NaF relative to 600 μM LiF. Lithium which can be beneficial for some organisms lessened the adverse effects of F^- or was less toxic than equimolar Na^+. Additionally, only 1,000 genes responded to LiF whereas close to 2,400 genes responded to NaF.
- The large number of genes that responded (i.e., 2,400 genes for sprayed pH 6 solutions with 600 μM NaF (only) vs. 320 genes for sprayed pH 6 solutions containing 100 μM U + 600 μM F) suggests that aqueous complexation of $U(VI)O_2^{2+}$ with F^- (such as $UO_2F_4^{2-}$ which was most likely at pH 6) may have lowered U+F bioavailability. This aqueous complexation between U and F and/or precipitation of a U(VI) oxide hydrate may have limited plant uptake. Conversely, most all of the genes that responded to 600 μM Na- or Li-based F^- also responded in the pH 3, 100 μM U + 600 μM NaF treatment and not in the pH 6, 100 μM U + 600 μM NaF treatment. This suggests that the effect of F^- on the plant shoot gene expression may have been diminished due to the complexation of F^- with U(VI). About 20 genes responded to the pH 6, 100 μM U + 600 μM NaF treatment and no other treatment.
- Several tens of genes responded to exposure from 600 μM LiF and no other treatment and several hundred genes responded to the 600 μM NaF and no other treatment condition.

The plant shoots in this study responded in a unique and statistically-significant manner to each type of treatment condition. This revealed that the sprayed contaminant solutions were able to interact with the plant leaf tissue and influence the omics responses for at least a week after treatment. The aqueous solution speciation chemistry was deemed important because it potentially influenced the biological availability of the added contaminants. The length of the post-exposure growth period as well as the initial contaminant concentration level had considerable influence on the plant omic response within the TRANS datasets.

Source Attribution of Atmospheric Radionuclide Emissions From Signatures Embedded Within Varying Background Signals

Steven R. Chiswell, Robert L. Buckley, Robert J. Kurzeja, David W. Werth

Source attribution by sampling downwind radionuclide concentrations can be problematic if the signal of interest is superimposed on a background signal with fluctuations of comparable magnitude. However, detection sensitivity can be greatly enhanced if we consider the differences between the power spectrum of a close-in source versus that of the global background - the latter concentration is well-mixed with long period variations in space and time, whereas close-in sources are characterized by a high frequency signal. Observed data and the background environment were analyzed to demonstrate source attribution using a wavelet transform. A mesoscale model was used to simulate release events which could be sampled and compared to observational data while a global transport model was used to model background concentrations using known emission sources. To determine how well the analysis can reveal an emissions source, simulations comprising a hypothetical emission source and observations from multiple locations were combined to develop a multiple source-receptor method for signal attribution.

The detection of radionuclide emissions from clandestine sources is a key component in any non-proliferation monitoring framework which must be able to discriminate these emissions from ubiquitous background concentrations. Large reprocessing facilities contribute significantly to the increasing global background concentration, while the typical proliferation facility is relatively small and the emission rates are potentially episodic as well. In addition, radioisotopes in commercial use (e.g., medical isotopes (MI), nuclear power plants (NPP), etc.) contribute to the background signal and further complicate the task of separating the proliferant signal from the background. Experience has demonstrated the need for robust determination of uncertainty during: high background variability; weak signals and limited sampling; and guidance on how to reduce the uncertainty with limited additional resources. The combination of signal processing with numerical modeling will enable greater use of high precision, low counting capabilities. Traditional avoidance of false alarms has required the use of a large standard deviation factor to ensure the measurement exceeds the background environment at the expense of generating a small probability-of-detection. The results obtained from this project demonstrate that signal detection is possible even when background variability is larger than the range of the proliferant.

Global concentrations with output every 3 hours for 2012 based on inventory of NPP and MI emissions were modeled using updated operating conditions as existed for the period. High resolution Regional Atmospheric Modeling System (RAMS) simulations of tracer releases from known sources and hypothetical ‘unknown’ sources were used to compute an index for plume overlap. Identification of an unknown plume when sources are mixed is complicated by background variability. Fourier analysis of modeled concentrations for locations in Japan revealed 17-20 hour spectral peaks which were traced to NPP sources in South Korea. Modeled spectral signals are consistent with peaks detected in radiation measurements obtained from Japan Nuclear Regulation Authority System for Prediction of Environment Emergency Dose Information (SPEEDI). Wavelet analysis of 2012 SPEEDI data was performed for 9 Japanese locations. The wavelet transform, unlike the Fourier transform, enables spectral components and their time of occurrence to be combined in source identification.

Results from this project show that atmospheric modeling of the background environment is capable of differentiating a nearfield plume from the background utilizing spectral frequency. In particular, our results have shown that the signal from a point release broadens in space and time with downwind transport distance and also loses its high-frequency component. A wavelet analysis of real-time observations (Figure 1) was developed to separate signals according to wave number and therefore identify potential sources for plumes with contributions from multiple sources while a multiple source-receptor regression model was developed utilizing input from high resolution model simulations and observed radiation measurements to determine significance of unexplained variance in order to improve source attribution from suspected or unknown sources.

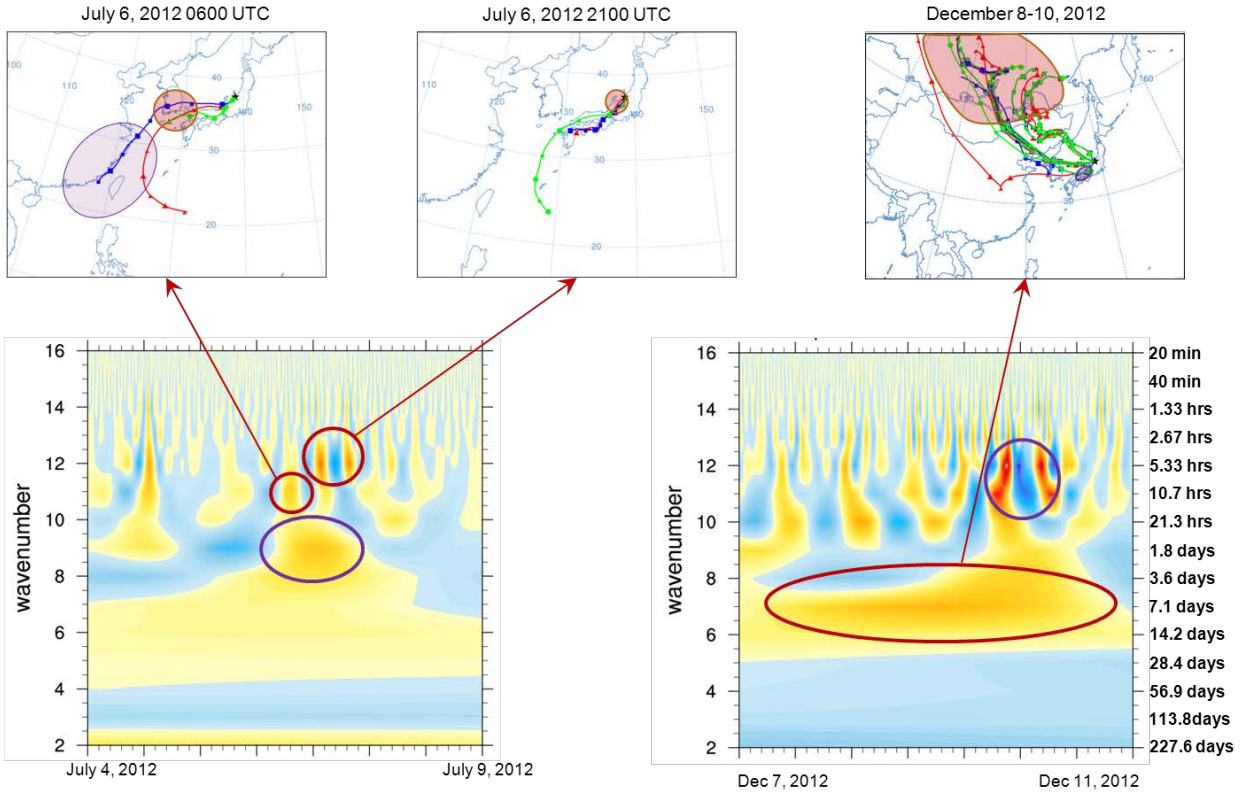

Figure 1. Wavelet spectra for July 4-9 (left) and December 7-11, 2012 (right) at Niigata, Japan. Computed back trajectories (top) depict wave number dependence on source region. Peaks in the wavelet power spectra (circle areas) are associated with sources (shaded regions along back trajectories). Lower wave number peaks represent contribution from sources at greater distances.

Global and regional models were able to reproduce realistic radionuclide signals which can be analyzed to determine wave spectra. Sources located further away from the sample location will contribute to lower wave numbers while nearby sources will contribute to high frequency wave numbers. Fourier analysis demonstrated numerical models were able to reproduce signal characteristics in observed measurements. A wavelet analysis was used to determine the wave spectra for 2012 at SPEEDI locations. The wavelet analysis can be used to classify known source regions according to wave number. Output from high resolution model simulations can be used to quantify the unique plume contribution from multiple overlapping sources. A multiple source-receptor regression model was developed to quantify significance of unexplained variance in observed data when compared to model predictions from existing/known sources. The shutdown of Japanese nuclear power reactors in the aftermath of Fukushima enabled comparison of atmospheric signals using available monitoring which may be analyzed prior to, and after the July 2012 restart of the Ohi NPP.

Photonic Crystals for Enhanced Light Outcoupling of Scintillation Based Detectors

Ricardo D. Torres, Lindsay T. Sexton, Roderick E. Fuentes, José Cortes-Concepción, Goutam Koley, Luiz Jacobsohn

The sensitivity of scintillation based detectors is maximized with increased photon yields. These are critically limited by total internal reflection within the crystal, leading to an undesirable decrease in the energy resolution of the counter. In this work we studied the use of photonic crystals (PhCs) to minimize total internal reflection in high refractive index scintillators. Efficient light extraction is achieved through periodic 2-dimensional nanoscale patterns, which inhibit light propagation along directions transverse to the surface. A computational technique was used to design a PhC pattern yielding a full photonic band gap for an indium tin oxide / bismuth germanate system. A convenient and low-cost approach was then investigated for PhC preparation by adopting highly-ordered porous anodic alumina membranes as selective dry-etching masks for pattern transfer. The light output yield of a PhC-modified scintillator is expected to be significantly increased relative to non-PhC structure.

Fig. 1. *BGO single crystal scintillator.*

Improved sensitivity of next generation scintillator detectors will be principally dependent on the system's energy resolution, ΔE, and timing resolution, Δt. The best ΔE of a scintillator detector is achieved with maximized photon yields and higher photoelectric cross sections, σ_{pe}, i.e. higher probabilities for capturing incoming radiation. Since σ_{pe} is proportional to the effective atomic number of the crystal ($\sigma_{pe} \sim Z_{eff}^{4.5}$), heavier materials result in a higher number of photoelectrons, N_{pe}, registered during the scintillation event. However, heavy materials have high refractive indices (n = 1.8-2.4) relative to the ambient medium (typically an air tight enclosure, n = 1). Therefore, as the scintillation light is emitted in all directions, only a limited fraction (~10-30%) is able to outcouple to the surface at which the photomultiplier tube (PMT) or other sensor is located. In this work we studied the use of photonic crystals (PhCs) for enhanced light outcoupling from single crystal scintillators. PhCs allow for efficient light extraction via 2-dimensional nanoscale patterns on the scintillator surface, which inhibit light propagation along directions transverse to the surface (i.e. create a photonic band gap). To date, large-area PhC scintillators have not been fabricated due to the impracticability and high cost of the only explored

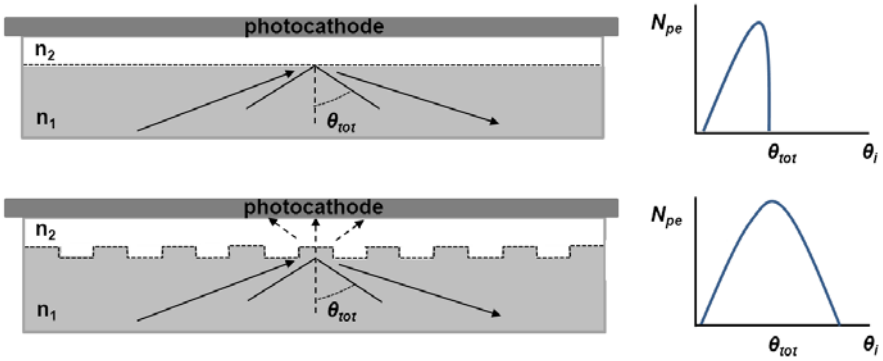

Fig. 2. *Light extraction from a scintillator (n_1) surface where $n_1 > n_2$ (air, vacuum, grease) for a flat surface geometry and a photonic crystal structure. Angular distribution of the photons effectively extracted from the scintillator surface.*

method, e-beam lithography patterning. This work, however, investigated the use of a convenient low-cost alternative by adopting highly-ordered porous anodic alumina membranes as selective dry-etching masks for pattern transfer.

Bismuth germanate (BGO, $Bi_4Ge_3O_{12}$, n=2.15 at 480 nm) was chosen as a model single crystal due to its widespread use in homeland security and medical imaging applications. The dispersion relations (band diagrams) of different PhC patterns were modeled on a single crystal coated with conductive and transparent indium tin oxide (ITO). The similar refractive index of ITO (n=2.07 at 480 nm) to that of BGO helps minimize scattering losses at the coating/scintillator interface, while facilitating the preparation (etching) and characterization of the PhC structure.

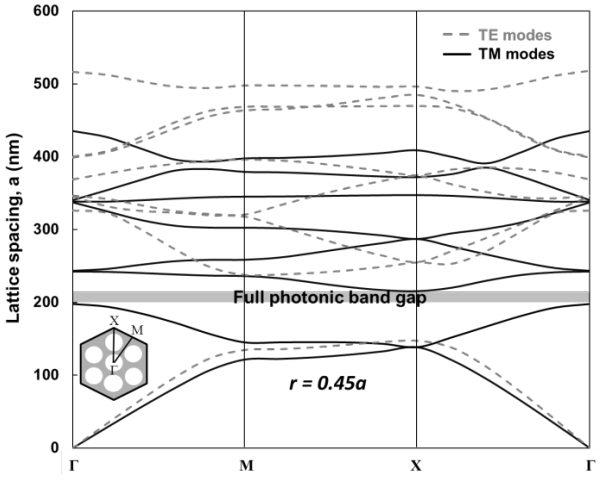

Fig. 3. *Dispersion relation of a photonic crystal scintillator (BGO) with a honeycomb hole pattern for a pore radius (r) to lattice constant (a) ratio of 0.45.*

An electrochemical process in a phosphoric acid solution was used to synthesize alumina membranes with dimensions closely matching the results of the frequency-domain computational model. The technique relies on the well-controlled anodization of a high-purity aluminum foil followed by detachment of the porous membrane in a saturated mercury chloride solution. The pore diameter and lattice pitch was controlled by a final widening step in dilute phosphoric acid. The anodized alumina membranes were then fixed onto BGO crystals by spin-coating with a dilute polymer solution. A parallel plate reactive ion-etching process was then used to investigate replication of the pore pattern onto the ITO-coated crystal. An alternative pillar-forming method for the fabrication of photonic crystals was also investigated. The membrane was mounted on the surface of a bare BGO crystals and ITO was sputtered to replicate pillars inside the pores. The alumina membrane was then dissolved in a dilute phosphoric acid solution to reveal the structure.

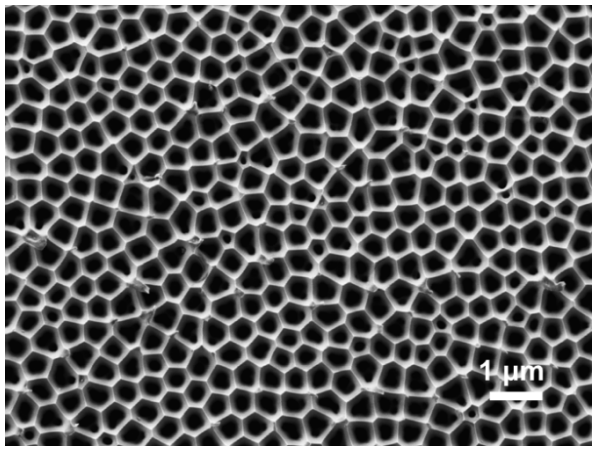

Fig. 4. *Scanning electron micrograph of highly-ordered porous anodic alumina masks prepared for the fabrication of photonic crystal scintillators.*

Baseline measurements were conducted to compare the luminescence response and light extraction efficiency of both bare and ITO-coated BGO single crystals. The spectra obtained with a ^{241}Am source (not α-blocked) showed a broad peak centered at higher channels (attributed to the energetic 5.5 MeV alpha particles) and a sharp peak at lower channels (attributed to the 60 keV gamma rays emitted by the source). The higher channel shift in the peaks for the bare crystal indicated an outcoupling loss as a result of the coating. Additional

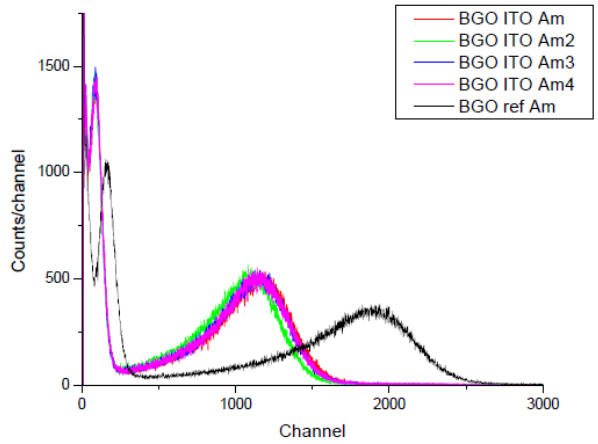

Fig. 5. *Scintillation spectra from bare and ITO-coated BGO single crystals (^{241}Am source, not α-blocked, 60 s integration time, no grease used for optical matching).*

work is required to characterize the effect on the luminescence response from the photonic crystal structure on the ITO coated sample.

A new technology in α-γ and β-γ coincidence counting

Tad Whiteside; Madeline Basile; and George King

Abstract: *We built and tested a prototype digital liquid scintillation coincidence spectrometer capable of characterizing radio nuclides (RN) in a complex matrix. This new design uses α-γ and β-γ coincidences to uniquely identify specific RNs of interest, effectively removing the background from other RNs. The digital system records all of the events that are detected into a binary data file, and allows examination of each recorded event, check for coincidence, and evaluate coincidences against known α-γ or β-γ energies to determine the decaying RN. In addition, coincidence methods can be used to determine disintegration rates for each RN without efficiency calibrations. This method effectively eliminates partial energy background events and external background events and characterizes all α-γ and β-γ RNs in a sample. This prototype system is the first step towards a compact field deployable system that could be used in a mobile laboratory or as part of a larger automated sample testing system.*

Isotopic identification is a challenge when using traditional liquid scintillation detection due to its susceptibility to β and gamma backgrounds and poor energy resolution when multiple α emitting isotopes are present. The background and resolution issues have been overcome by SRNL researchers. They developed an analog α/β-gamma coincidence spectrometer system that uses an Ordella PERALS unit to discriminate between α and β radiation and provide a coincidence gate for a γ spectrometer. This coincidence data is used to identify the nuclides within the sample; however, in a multi-nuclide sample, identifying additional nuclides requires re-running the sample (at a minimum of 4 hours per nuclide) and manually changing the coincident gate settings. The digital system built in this work records all of the data during a single sample acquisition and the identification of additional nuclides only requires re-analysis of the data file (less than 1 minute per nuclide). Due to the single sample acquisition and rapid data analysis, this digital system will facilitate identification and measurement of radionuclides in the field. In addition to this primary objective, this work has advanced the SRNL knowledge of digital data acquisition systems and signal analysis software programing. Finally, this work was the necessary next step towards creating a commercial detector system using this technology.

The creation of the digital spectrometer system required work on both the hardware and software side. On the hardware side, the alpha spectrometer was modified to read signals directly from the photomultiplier tube (PMT). To identify the coincident events within the data file, we had to measure the time delay between the alpha signal detection and the gamma signal detection. Once the hardware was setup, the signal detection from the detectors had to be optimized. This portion of the project was assigned to a Department of Homeland Security summer intern. She read the technical literature on the digital acquisition system and learned how to modify the gain, and the trigger and energy filters to maximize the energy resolution and minimize the noise in the output signal. After the signal output of both detectors was optimized they were energy calibrated.

On the software side, in order to (re)analyze the data file, being able to quickly read and manipulate the data file was of utmost importance. To accomplish this, a rapid parsing program was created to read and parse the binary data file. This parsing program was two-orders of magnitude faster than the

vendor supplied parsing library. After the data was read, additional software was created to analyze and visualize the detector data and the coincident events. The coincident events were determined by the width of the experimentally determined coincidence window. The results of the analysis are presented in a graphical user interface which shows the 2D histogram of the energy spectra and the 3D histogram of the coincident events.

A pulse shape analysis (PSA) algorithm that discriminates α particles from β particles was developed. This algorithm is based on the fluorescence of the particles (α particles cause the scintillation cocktail to fluoresce for longer than β particles), and the associated pulse widths from each type of particle, see Figure 1.

The disintegration rate of the nuclide of interest can be determined without the need for detector efficiency calibrations through the use of coincidence counts. The formula used is $A = c_1c_2/(c_{12} - c_r)$ where *A* is the activity, c_1 is the count rate of the γ detector, c_2 is the count rate of the PERALS, c_{12} is the coincidence count rate, and c_r is the random coincidence rate. To determine the activity, a window is defined around the energies of interest in both the PERALS and gamma spectra and the count rate in each window is measured as well as the actual and random coincident count rates. From these rates the activity is measured.

Once the hardware and software components were developed, they were tested through a series of data acquisitions and analysis. The output of one of the data acquisition and analysis of Am-241 can be seen in Figure 2.

This project was successful in that we met our primary objective of highly resolved, rapid data acquisition and analysis. We can distinguish individual coincident events and determine the activity of the samples.

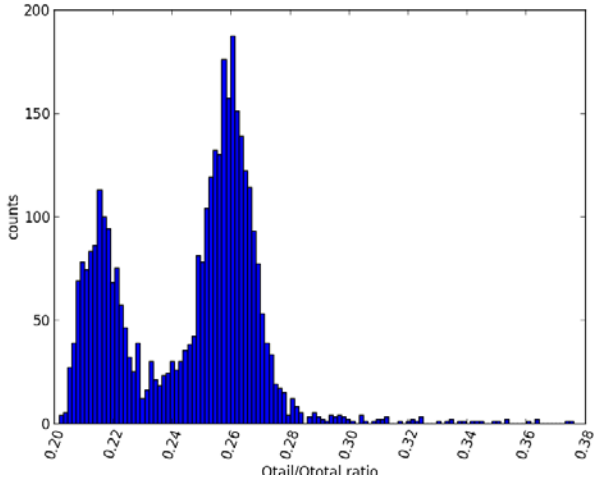

Figure 1. Alpha-beta separation in Ra226.

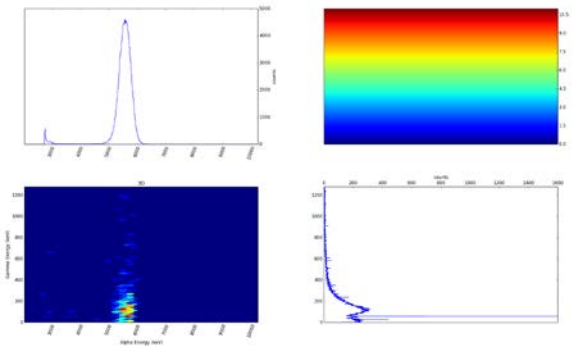

Figure 2. Am241 acquired for 40 minutes.

Optical Monitoring of Canister Environments in Dry Cask Fuel Storage Systems

Robert Lascola, Patrick O'Rourke, Charles Crawford

This work explores the feasibility of using optical methods for monitoring conditions inside dry cask fuel storage systems. These methods can supplement existing devices by providing information on chemical species that are markers for chemical degradation processes. Examples include N_2 to indicate air leaks and $O_2/H_2/H_2O$ to indicate corrosion potential. Necessary components to any optical system, such as windows and multipass cells, must withstand the high radiation fields and elevated temperatures in the casks. Therefore, we have evaluated a number of Ce-containing glasses from the Si-Mg-Li and P-Al families, as well as polycrystalline diamond windows, for changes in color and structure when exposed to $>10^8$ rad. We have also demonstrated the ability to detect N_2 and O_2 through these glasses using an optical fiber Raman probe and reflecting mirror. Results indicate that the optical detection scheme is feasible.

This work addresses high priority gaps regarding advanced, nondestructive, and nonpenetrating monitoring and instrumentation capabilities identified for the support of relicensing efforts pertaining to extended storage of used nuclear fuel.[1,2] These capabilities should provide for "early detection of confinement boundary degradation, monitoring cask environmental changes, and data transmission without compromising cask or canister boundary".[1] Existing methods provide data on temperature, pressure, mechanical integrity, and ^{85}Kr (the latter by sample extraction). However, needs based on molecular analysis do not yet exist. Detection of H_2O (either directly or as the radiolysis products H_2 and O_2) would provide an indirect measure of corrosion potential. Detection of N_2 would indicate air leaks into the He cask atmosphere. Optical methods, particularly Raman and IR spectroscopies, can provide this information, if there is a way to introduce light into the casks and collect it for spectral analysis. Development of methods that will work in this high-radiation and elevated temperature environment would be a unique capability. The technical objective of this work is to demonstrate that such methods are feasible and to start building a prototypical system.

Our methodology was to investigate the two absolute requirements of an optical measurement scheme. The window (and other optical components) must be suitably resistant to radiation and temperature exposure over the lifetime of the canister, and the analytical measurements must be sensitive enough to be useful for diagnostic purposes. We investigated several potential window materials based on cerium doping of SiO_2-MgO-Li_2O or P_2O_5-Al_2O_3 glasses. Ce^{3+} is known to suppress the darkening of glass by ionizing radiation, though at the cost of coloring the base color of the glass.[3] These particular formulations allow higher initial Ce content without coloring. We also investigated samples of polycrystalline diamond windows produced by chemical vapor deposition. Although more expensive than traditional glasses, this material has advantages of hardness and optical clarity. We exposed samples to total doses of γ radiation (^{60}Co source) $>10^8$ rad, examining at intermediate exposures UV-visible-NIR, Raman, and IR spectroscopies, and physical appearance. We also set up a simple reflection

[1] B. Hanson *et al., Gap Analysis to Support Extended Storage of Used Nuclear Fuel,* FCRD-USED-2011-000136, Rev. 0, U.S. Dept. of Energy, January 31, 2012.
[2] B.D. Hanson, *Used Nuclear Fuel Storage and Transportation Data Gap Prioritization,* FCRD-USED-2012-000109, U.S. Dept. of Energy, April 30, 2012.
[3] J.L. Rygel and C.G. Pantano, *J. Non-Crystalline Solids*, **355**, 2622-2629 (2009).

cell comprised of an optical fiber Raman probe and spherical front-surface Al coated mirror. We placed the glass samples in front of the probe and measured Raman scattering of O_2 and N_2 within the cell.

The most notable effect of irradiation was on the absorbance spectroscopy and visual appearance of the glasses. Results are summarized in the figure. Despite high (3%) Ce loading and being initially colorless, darkening of the Ce-P-Al glasses continued to increase through 6.8 x 10^8 rad. In contrast, darkening of the Si-Mg-Li glasses plateaued at ~5 x 10^7 rad – well below expected cask doses despite lower (1%) Ce and an initial amber color. Polycrystalline diamond remained clear for all doses; however, the high refractive index led to reflection losses approaching 40%.[4] Despite the darkening, all glasses remained transmissive at wavelengths above 500 nm, suggesting that Raman spectra could be taken through the windows (excitation at 532 nm and scattering at 540-690 nm).

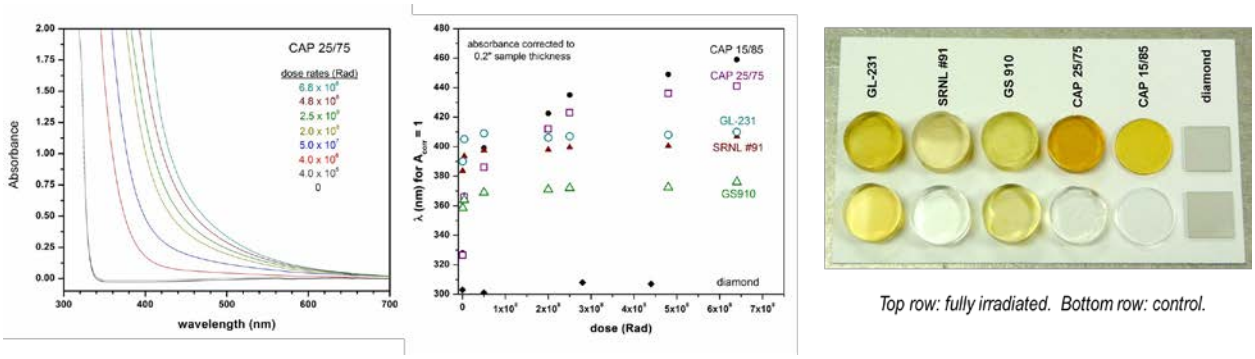

Raman and IR spectra of the windows themselves were invariant with increasing dose, indicating no major structural changes. There were no Raman peaks above 1500 cm^{-1}, allowing detection of N_2, O_2, and H_2O gases. All glasses had transmission ≥ 50% at wavelengths < 2.7 μm (3700 cm^{-1}), which is suitable for observing H_2O vapor.

The retroreflecting cavity yielded >3x signal for atmospheric N_2 and O_2 compared to the signal from the probe by itself. N_2 and O_2 were also observed through all γ-exposed windows. The optical setup was not ideal – a longer probe focal length would reduce the relative Raman signal from the windows – but these measurements demonstrated the feasibility of optical monitoring.

This work demonstrated that Ce-doped Si-Mg-Li glasses are good candidates for windows for dry cask storage containers. Although initially amber, these glasses do not darken substantially upon exposure to γ radiation in excess of 5 x 10^7 rad. Ce-doped P-Al glasses are initially clear but the full extent of γ-induced darkening is not known. Polycrystalline diamond is unchanged at high doses, but cost and high reflection losses could limit where this material is used. All potential window materials support the use of Raman and IR spectroscopy to detect molecular gases that are indicators of important degradation processes inside the containers. Successful measurements of O_2 and N_2 using a retroreflection cavity show the feasibility of measuring the cask interior with these windows, although more sensitivity will be required to meet measurement requirements.

[4] These losses could be mitigated with index-matching anti-reflective coatings, although the resistance of the coatings to high rad doses would have to be evaluated.

A Novel Method for Determining Strontium and Actinide Decontamination Factors of Sodium Titanates

Simona E. Murph
Kathryn Taylor-Pashow
F. F. Fondeur
D. T. Hobbs

Three different metal-impregnated sodium titanate sorbents were prepared that provided surface-enhanced Raman scattering (SERS) responses, which correlated with plutonium uptake. In contrast to the conventional method, this technique provides a rapid, in situ method to measure actinide and strontium decontamination factors (DF).

The objectives of this project are two-fold, (1) synthesize functional sodium titanates that can sorb actinides and strontium and (2) that the functional material exhibit an enhanced Raman scattering that allows detection of the loaded actinide and strontium. The project examined two different metal-sorbent configurations, (1) surface decoration of the sorbents with nanometals of different geometries and (2) nanometallic cores covered with a sorbent layer or shell. Having a SERS sorbent provides the opportunity to determine adsorption by an in situ method that is cheaper, faster, and reduces personnel exposure compared to conventional methods. In the conventional method, an aliquot of the reaction mixture is removed from the test, the solution and solids phases are separated by filtration or centrifugation, and the solution is analyzed by an appropriate analytical technique. The difference between the initial sorbate concentration and that measured after some time interval is that assumed to have sorbed/exchanged onto the solid phase. Analysis of the solids, if pursued requires additional handling prior to analysis.

Using wet chemistry techniques several functionalized sorbents were prepared of which the composition and method synthesis is proprietary at this time.

Samples of the functionalized nanosorbent were contacted with a salt solution containing strontium and actinides. The resulting mixtures were analyzed in a Raman microscope equipped with a 785 and 532 nm lasers. The broad peak at 810 cm^{-1} is believed to be due to the interaction of plutonium with oxygen atoms on the titanate sorbent. This peak is several wavenumbers shifted down from the 930 cm^{-1} peak expected for the “oxo” specie in solution.

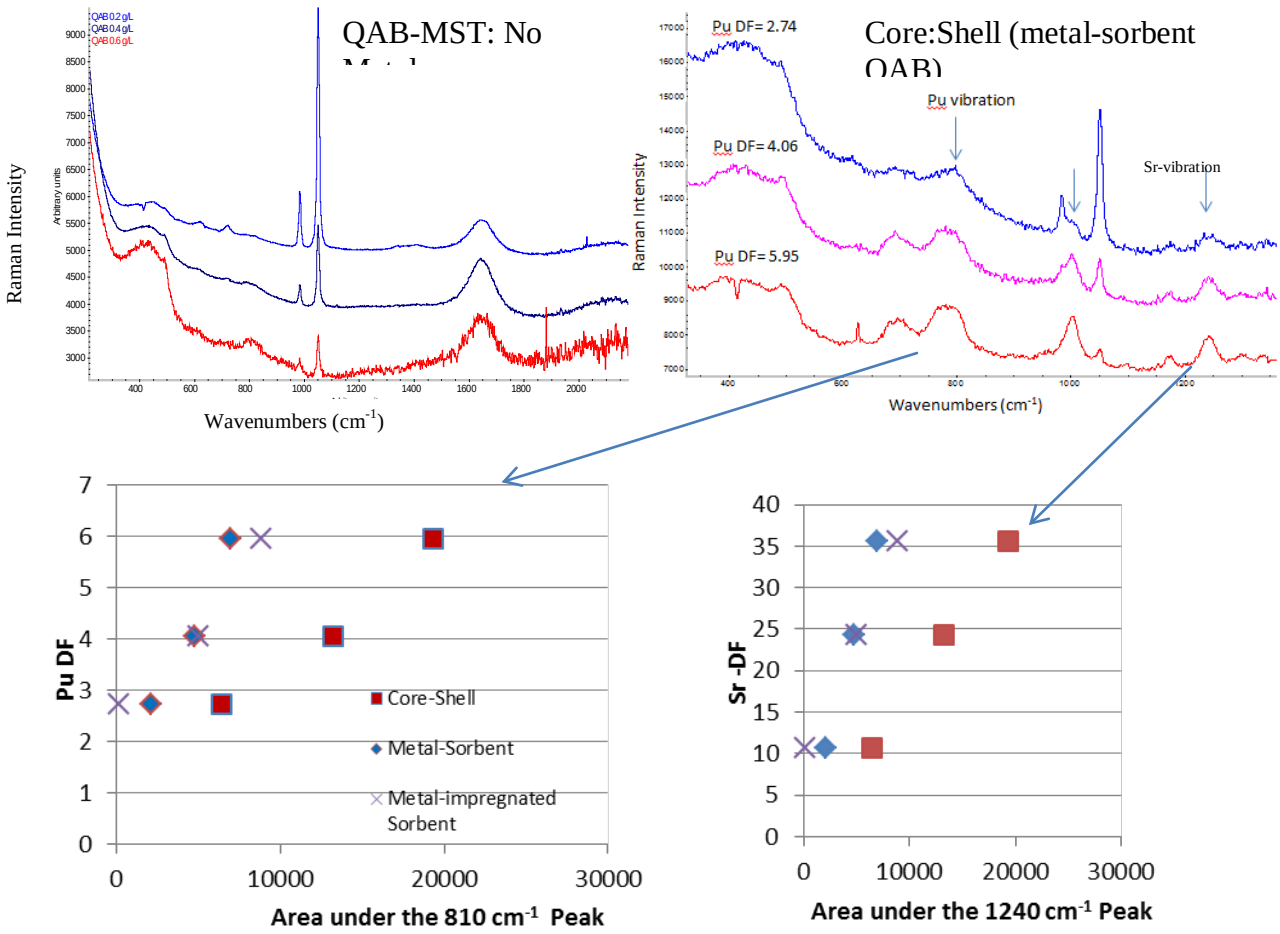

Figure 1. A plot of the Pu Raman peak versus Pu and Sr decontamination factors for core-shell nanosorbent at three different concentrations. Upper left inset is the Raman spectra of MST without metal but loaded wth Pu and Sr.

Figure 1 shows a summary of the data obtained from the three different sorbents evaluated in this work. As can be seen from this figure, the area under the peak around 810 cm^{-1} assigned to one of the Pu-titanate interactions changes linearly with the decontamination factor for Pu determined by the conventional technique. This means that the Raman signal at 810 cm^{-1} can be used to determine the amount of loaded Pu and thus, the Pu DF value. A less dramatic effect was observed in the samples decorated at the surface with nanometals (diamond and cross data in Fig. 1). The data indicate the core-shell configuration maximizes the SERS responsive effect. The peaks at 1170 and 1240 cm^{-1} are believed to be associated with Sr on the sorbent (Sr-OH bend) and their signal at 240 cm^{-1} (area under the peak) correlates linearly with Sr decontamination factor.

In conclusion, the project successfully made novel and functional nanosorbents that can sorb actinides and strontium and produce an enhanced Raman response. The observed Raman response (at 810 cm^{-1} and 1240 cm^{-1}) was linearly related to the amount of Pu and Sr loaded onto the sorbent. The core-shell configuration showed the greatest Raman response for the determination of the Pu and Sr DF values. Therefore, we demonstrated a rapid, insitu method that can successfully determine Sr and Pu DF values.

Porous Rhenium Nano-Structures for Thermal Ionization Mass Spectrometry Filament Enhancement

Brian Ticknor, Steven Serkiz, Charles Shick, Jr., and Jay Gaillard (SRNL)
Jian He, Rama Podilla, Jingyi Zhu, and Apparao Rao (Clemson University)

Abstract: *Porous rhenium (Re) nano-structures were produced in the laboratory to determine if these nano-structures could increase sample utilization efficiency for thermal ionization mass spectrometry (TIMS). Porous rhenium nano-structures were produced with different sizes, thicknesses, porosities, and nano-structure sizes; however, the attachment of these nano-structures to traditional rhenium TIMS sample filaments proved difficult. Efforts to produce porous rhenium nano-structures long enough to fabricate TIMS sample filaments also did not work. Some TIMS research has indicated that carbon materials can increase the thermal ionization mechanism if rhenium carbide can be formed on the traditional rhenium TIMS filament. Pieces of carbon nanotube yarn and pieces of vertically aligned multiwalled carbon nanotubes were added to traditional rhenium TIMS filaments. No sample utilization efficiency gains were observed for a small sample set with these nano-structured carbon materials.*

Technical Objective/Significance: The measurement of lanthanide and actinide isotope ratios, especially for very small sample sizes (ng to fg, depending on analyte of interest), is a vital tool for nuclear counter-proliferation and safeguard activities. Thermal Ionization Mass Spectrometry (TIMS) is generally accepted as the state of the art technology for ultra-low level measurements of these actinide ratios. Currently, the efficiency of a typical TIMS instrument represents the detection of <0.5% of the total number of atoms loaded into the instrument. This fairly poor sample utilization efficiency creates significant room for improvement, and even a small enhancement in TIMS performance would represent a significant gain in sensitivity.

Previous work within the DOE complex has shown that micro-scale porous ion emitters (PIEs) fabricated from micron-sized rhenium powder produce ionization from a point-like source rather than traditional TIMS filaments, leading to better focusing of the ion beam through the instrument and increasing the sample utilization efficiency. Our research was to examine the extension of this finding to filaments which were added porous rhenium nano-structures or to fabricate TIMS filaments with porous rhenium nano-structures. Within this period of performance, the attachment of these nano-structures to traditional TIMS filaments proved difficult, and the efforts to produce porous rhenium nano-structures long enough to fabricate TIMS sample filaments also did not work. Other work explored the addition of nano-structured carbon materials.

An instrument baseline for low level plutonium samples was established for traditional resin bead sample filaments for the Nonproliferation Technologies Section (NTS) IsoProbe-T thermal ionization mass spectrometer. A comparison of the current NTS method and the purposed enhanced filament method was hoped with this instrument baseline. This instrument baseline will be helpful for future sample utilization efficiency research projects.

Research Methodology: Specific steps conducted for this research were (1) to develop synthesis approaches to produce porous rhenium nano-structured materials; (2) to add these nano-structures to traditional TIMS filaments; (3) to compare these "enhanced" filaments with current NTS method for low level plutonium samples to determine if sample utilization efficiency changed. The attachment of these

porous rhenium nanostructures proved difficult so efforts to fabricate TIMS filaments containing the nanostructures produced in step (1) were pursued. The porous rhenium nano-structures could not be fabricated into viable TIMS filaments.

Three approaches were examined in the synthesis of rhenium nanostructured materials. The approaches were: spark plasma sintering (SPS) of rhenium powders; acid etching of rhenium solids (both commercial wire and samples produced by SPS process); and laser ablation mediated synthesis (LAMS). An SCUREF contract was written to Jian He and Apparao Rao of the Clemson Physics Department to conduct the synthesis under the direction of the principle investigators on this project. Unfortunately, the start of work was postponed from March 4th to May 27th due to concerns by Clemson University Export Control Office.

Results/Discussion: In general, the SPS process profoundly affects the sintered materials by means of wandering spark plasma, electric field, self-adjusting electric current distribution, and intensive heating/cooling processes in the interfacial boundaries. The combined effects could help make advanced materials that cannot be realized otherwise, for example, densification of nanomaterials and nanocomposites. In particular, the presence of spark plasma and the intensive heating in the interfacial boundaries aid in the fabrication of advanced materials and novel phases. Commercially available rhenium powders from Re Alloys Inc. were used as starting materials in the SPS process and the current and cycle time (temperature) and pressure of the SPS system were varied in order to produce rhenium bars and varying porosity, morphology, and mineralogy.

SPS was run on rhenium powder under varying conditions, and materials were produced with the final porosity of the resulting solid from 57 to 86% of rhenium metal. The solids produced by SPS turned out to be difficult to add to traditional TIMS filaments and to fabricate into filaments due to brittleness and hardness making mechanical cutting impossible. Therefore, simple nitric acid etching was investigated on traditional rhenium filament materials as a means of adding porosity and surface area to the filaments. Acid etching was conducted on SPSed rhenium powder (1300 ˚C for 5 min), 0.1 mm rhenium wire, 0.25 tungsten-rhenium wire, and a commercial TIMS rhenium filament used by SRNL. These acid etching materials could not be fabricated into TIMS filaments either.

SPS Temperature (°C)	SPS Pressure (MPa)	SPS hold time (min.)	Density (g/cc)	% Theoretical density
800	10	5	12	57%
1000	10	5	15.7	75%
1200	10	5	18	86%
1480	10	3.5	18	86%

Nanoparticles prepared by LAMS from rhenium foil exhibited a hydrodynamic size is ~217 nm and a zeta potential of -29 mV indicating moderately stable suspension. Nanoparticles prepared by ablating the SPSed pellet exhibited a hydrodynamic size is ~226 nm and zeta potential of -27 mV indicating moderately stable suspension. None of these nanoparticles were shipped to SRNL since stable suspension targets were not reached.

Conclusions: Porous rhenium nano-structures were produced by several techniques. However, the addition of these nano-structures to traditional TIMS filaments was difficult. The fabrication of filaments from the porous rhenium nano-structures was also difficult for evaluation with the instrument baseline for low level plutonium samples by the current NTS TIMS method. No enhanced sample

utilization efficiency was observed for the addition of nano-structured carbon materials to traditional TIMS filaments. Further work is still needed for TIMS sample utilization efficiency.

Authenticated Sensor Interface Device

Rick Poland, Bob Drayer, Jason Wilson

A primary goal of the International Atomic Energy Agency (IAEA) is to ensure nuclear materials are used only for peaceful activities and are not diverted for undeclared activities. The collection of authenticated material balance information from operator instrumentation is a concept that will allow the IAEA to cost effectively move toward the stated goal. Currently the IAEA has no capability to securely monitor operator instrumentation. The Authenticated Sensor Interface Device (ASID) can perform this function and become a key component of the IAEA to cost effectively attain the goal.

The ASID project researched requirements, techniques, and components for ASID, then designed, implemented, and tested the ASID prototype which is a micro-computer based device with custom hardware and software that interfaces to a typical nuclear material accountancy scale. The ASID prototype provides the ability to share data among a number of parties while ensuring the authentication of data and protecting each party's interests from attack.

The objective of the Authenticated Sensor Interface Device (ASID) project was to research the requirements for the device, research components and techniques required for development, and ultimately develop and test a prototype ASID that implements the basic functions of the requirements, for example securely sharing authenticated data and protecting each party's network from attack. By developing an ASID prototype, SRNL will provide the basic component for the IAEA to collect authenticated safeguards information from operator instrumentation, which may include accountancy scales, load cells, nondestructive assay (NDA) instrumentation, and other safeguards related equipment for international safeguards applications. As the IAEA continues to seek to increase the efficiency and cost effectiveness of their operations, the ASID will provide a key component for the implementation of remote monitoring and the joint-use of equipment, thus reducing the number of onsite inspections and ultimately the cost of safeguards.

The team first researched IAEA documents describing the IAEA's desire to implement the joint-use of nuclear process monitoring instrumentation to share safeguards related information with the operator. This research along with conversations with IAEA personnel also confirmed the IAEA's concerns regarding vulnerabilities of networks, data, and sensors to malicious attack. The team also consulted industry experts for feedback on the ASID concept before moving forward with the development of the initial prototype.

The team researched a number of technical areas prior to beginning the development of the ASID prototype. These areas included:

- Concepts to Share Yet Protect Data – Existing data diode solutions provide only unidirectional protection, and therefore are not suited for joint-use applications. The ASID team developed a concept which incorporates a "smart" interface in the form of an embedded controller that interfaces with the sensor, thus permitting both parties to be isolated from the sensor as well as the other party's network. (Figure 1)
- Encryption Methods – The team researched industry standard encryption techniques and developed software to implement encryption algorithms on the embedded controller shown as

the data aggregate on Figure 1. Independent encryption was implemented for each party to further ensure no data manipulation or security breaches occur.

- Authentication Methods – Authentication methods were evaluated and a sign and forward technique was implemented. Further development is anticipated to develop a technique to implement PKI methods to simplify the field setup of the authentication scheme.
- Selection of Embedded Controllers – The ASID uses three embedded controllers, one data aggregate and two transmitters. These controllers were selected to compliance with requirements with limited capability for enhanced operation due to budget and time constraints.
- Communicating with Accountancy Scale – As the ASID is to be demonstrated with the Wohwa Accountancy Scale, software was developed to interface the data aggregate embedded controller with the scale electronics module.

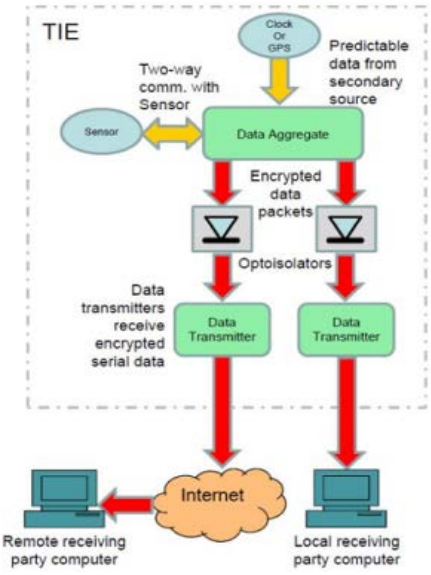

Figure 1

Based on the research discussed above the ASID prototype was design. All components were fabricated on a custom printed circuit board, the custom software loaded, and the ASID tested. After final on-board software development the ASID is performing all basic functions properly. The ASID printed circuit board has since been properly packaged for presentation and demonstration.

The development of the basic ASID prototype has been a tremendous success.

- The ASID is functionally operational with the Wohwa accountancy scale.
- SRNL filed a patent application (SRS-12-004) for ASID on November 1, 2012.
- Mr. Poland presented a technical paper on the ASID at the ANS/INMM sponsored 9th International Conference: Facilities Operations – Safeguards Interface.
- Mr. Poland presented a technical paper on the ASID at the 54th Annual Meeting of the Institute of Nuclear Materials Management.
- The ASID was demonstrated at SRNL's booth at the 54th Annual Meeting of the INMM.
- Canberra Industries has expressed interest in licensing the ASID technology for inclusion in the development of instruments for the IAEA.
- ORNL is collaborating with SRNL in the development of a white paper to develop the concept for the application of ASID to an NDA instrument at the Pelindaba Nuclear Site in South Africa.

Although the initial ASID prototype development has been successful, completion of the ASID requires additional research and development. Research into more versatile high speed embedded controllers is necessary to implement industry standard communication protocols as well as encryption and authentication standards, and subsequently the certification of the ASID as a FIPS-140-2 certified device. Additionally, the development of a concept for PKI encryption keys is required to simplify the integration of the ASID into full IAEA operations. In the industry modularity and versatility are

important, so research into concepts to increase the types of inputs accepted by the ASID (analog and digital protocols) and the modularization of these options need to be developed over the coming years.

Spent Fuel Cask Fissile Material Assay by Collimated Gamma Neutron Sensing and Modeling

Sean Branney, Jason Wilson, Lindsay Sexton, Christopher Verst, and Braden Brown

The storage of used nuclear fuel is a major long term issue for DOE and with the recent Blue Ribbon Commission Report it is likely that dry casks will be the storage method of choice for the foreseeable future. SRS's experience in waste disposal and long term storage (L-basin) make SRNL an ideal location for the development of techniques to support DOE's goal. Additionally, the International Atomic Energy Agency (IAEA) has a strong need for a method to re-verify the contents of dry casks after a break in continuity of knowledge.

This project will develop a method of assaying the fissile inventory of nuclear fuels in dry cask storage through collimated gamma spectroscopy, neutron counting and modeling. Previous work on shipping casks at L-basin has shown that it is possible to identify several isotopes with high resolution gamma spectroscopy even through the considerable shielding of a transport cask. Coupled with neutron counting and with extensive modeling, it will be possible to determine the fissile content of nuclear fuel stored in dry casks.

The objective of this project will be to determine the fissile inventory of a cask containing used fuel from gamma spectroscopy and neutron counting without the need to open the cask. This will require extensive modeling to determine the gamma and neutron field around several different types of casks (including transport casks typically received at L-Basin) for different fuel burnups and configurations. Gamma spectroscopy will be used to quantify the amount of Cs-137 and Eu-154 in the fuel and other fission products, depending on the age of the fuel (Cs-134 for younger fuel). The use of neutron counting to confirm the remaining fissile inventory in conjunction with the gamma spectroscopy will be investigated.

The following questions will be answered by this project.

- With sufficient modeling, what signatures can be used to uniquely determine the burnup of used fuel in a cask? The initial approach will be to use the absolute amount of Cs-137 and the ratio of Eu-154 to Cs-137.
- What parameters of the fuel is it important to model precisely in order to accurately predict the gamma spectrum outside the cask. For example, is there a significant increase in precision if the individual fuel assemblies have their rods modeled, as opposed to considering the entire assembly as a homogenous gamma source (with a calculated spectrum)? This will aid in speeding up the inventory determination in future cases.

At completion, the goal of the project will be to have developed a suite of models that have been correlated to measured spectra, allowing for the determination of fissile inventory in a range of cask types with different irradiation histories.

We have constructed a Mathematica program to automatically generate ORIGEN S inputs for 21 fuel types, from PWR's and BWR's to Russian VVER fuel assemblies. These models were examined for different irradiation histories and discharge times. From these models we have used the results to write a program to automatically calculate burnup and discharge time from Eu-154 or Cs-134 and Cs-137 amounts at any time after discharge. This was done with different irradiation histories and we have determined that the irradiation history of the fuel has a small effect on the final burnup. What this means is, taking into account the refueling outages rather than considering three cycles as a single

irradiation step has very little effect on the measured burn up at later times. In conjunction we have created a full core model of the MIT Research Reactor and the Missouri University Research Reactor using SCALE. From this we have determined that PWR fuel is easier to model than research reactor fuel because of the irregular power history with each individual fuel assembly. After the fuel isotopics were calculated with these models we then modeled (MCNP) a BRR shipping cask with MIT Research Reactor Fuel and a NAC-UMS dry storage cask with Westinghouse 17x17 fuel. Measurements have been performed on a BRR shipping cask with MIT fuel at L-Basin. It was determined that the gamma signatures alone that could be observed even through shielded casks would be sufficient for making the determination of burnup and discharge time without the need for neutron measurements.

The results of the modeling and experiment have shown that it is very plausible to calculate the amount of Cs-137, Cs-134 and Eu-154 present in reactor fuel at any time after discharge and extrapolate this back to determine its discharge time, and burnup (typically with other methods, one of these things has to be assumed) and a robust method for making this determination has been developed. Complications in the individual irradiation history of assemblies make it difficult to make this determination outside a cask, however. This is particularly the case with research reactor fuel where large variability in power histories are important and the proximity of individual fuel elements to control rods also has an effect. These effects are much smaller in PWR fuel which, by design, tends to have very averaged irradiation history (due to the desire to uniformly utilize fuel). However, given the number of assemblies in a fuel cask containing PWR fuel (one type, for example, holds 26 assemblies), deviations in individual assemblies will be hard to resolve from the aggregate burnup. This technique has a number of applications other than trying to measure assemblies through a cask. One of which would be verifying CANDU type fuel where it is customary for IAEA instruments to measure individual assemblies when they are discharged from the core, although the instrument is merely checking that the assembly has been irradiated. This method would allow for an straight forward determination of the assembly's irradiation history which would be particularly valuable in determining if it had been used for Pu production, for example via inserting a DU slug during irradiation. There are also nuclear forensic applications for this method.

Fast Neutron Directional Detection by Innovative Moderator Design

David DiPrete, Alex Couture, Hector Colon-Mercado, Matt Wellons, Mike Summer, Cecilia DiPrete

Conventional, commercially available neutron detectors typically consist of a thermal neutron detector such as a helium-3 tube surrounded by a neutron moderator material such as polyethylene. The incoming fast, high energy neutrons are moderated or slowed down by the moderator material so that they can interact with the neutron reactive material of the thermal neutron detector and be detected. Such detector systems do not provide directionality information. This LDRD explored the feasibility of designing a neutron detector capable of providing directional information so as to be able to more quickly identify the location of fissionable nuclear material emitting fast neutrons.

This directional fast neutron detector consists of a cubic neutron moderator coupled with a pair of neutron detectors located on opposite faces of the cube. That moderator-detector geometry is designed so fast neutrons would pass, undetected, through the closest neutron detector, then be moderated by the adjacent moderator surface, thermalized and finally reflected back to be detected by the adjacent detector. The moderator block itself shields the far neutron detector from seeing any neutron events. The far neutron detector is designed to measure ambient background, providing discrimination ability between real neutron events, and background events. The detectors' outer surfaces are covered in a thermal neutron shielding material (i.e. cadmium) to shield the detectors from ambient thermal neutron events. The detectors themselves for this LDRD project were envisioned to be silicon charged-particle detectors coated with a layer of (n,α)-reactive material, based on either Li-6 or B-10. This project aimed to develop the capability to generate such neutron reactive layers at SRNL. The focus of the project has been to use Monte-Carlo simulations to determine the ideal moderator and to deposit (n,α)-reactive materials onto silicon substrates testing their feasibility as neutron detectors.

Initially, the basic concept was tested. A 6x6 inch polyethylene moderator block was fabricated. He-3 tubes were positioned on one face of the moderator block and were shielded with cadmium. An Am-Li neutron source was positioned at various angles to the detector system. From this simple design, a directionality of 9 to 1 was established for neutron sources placed in front of the detectors vs when they were behind the detectors.

In determining the ideal moderator for fast-neutron directional detection, multiple MCNP simulations were then produced that had the following properties in common: (1) the moderator was a 6 inch cube, (2) two thin layers of B-10 were located on opposite sides of the cube, (3) a plutonium fission-spectrum neutron source uniformly irradiated one of the cube faces containing a B-10 layer, (4) the (n,α) reaction rate was calculated in each of the two B-10 layers. More than 50 different moderator configurations were modeled using different moderating materials, layers of neutron poisons or reflectors, and varying the temperature of regions of the block. Two figures-of-merit were used to compare the various configurations; the reaction-rate in the B-10 layer closest to the neutron source and the ratio of the two reaction rates. These figures-of-merit are related to the overall efficiency and directionality of the detection system, respectively. From these simulations, the optimum configuration was found to be a high-density polyethylene block with a 2-3 mm layer of cadmium along its central plane. The block should be surrounded by a 1-cm layer of nickel on any surface not covered by a detector. A 1-cm layer of polyethylene just beneath each detector face should be cooled to cryogenic temperatures. The cadmium increases the directionality, while the cooling and the nickel improve efficiency (cooling much more so). An 8-inch polyethylene cube was constructed and

coupled with He-3 tubes for laboratory testing of the directional detector concept. The detector was found to have a sensitivity of ±10° and the count rate varies by a factor of 9 between the near and far detectors. Unsuccessful attempts were made to improve the detector efficiency by cooling a layer of polyethylene using liquid nitrogen.

It turns out that there is an optimum thickness for (n,α)-reactive layers coupled to a charged particle detector. The charged particles emitted in this reaction lose energy as they move through the material towards the detectors. If the layer is too thick, then many of the charged particles produced will not be detected. If the layer is too thin, it will not capture as many neutrons. A cost-free online code, the Stopping and Range of Ions in Matter (SRIM), was used to determine the range of the charged particles in pure Li-6, Li-6 fluoride, Li-6 carbonate, pure B-10, and B-10 carbide. These ranges combined with thermal neutron cross sections were used to calculate the ideal thicknesses for these materials.

Rather than depositing these materials directly onto silicon detectors, the techniques were initially tested by depositing the materials onto silicon wafers. A small vacuum chamber was fabricated in the SRNL machine shop to hold a wafer one millimeter from the surface of a silicon detector. The vacuum chamber was placed on a polyethylene moderator along with an Am-Li neutron source for testing of the detector system. To test the gamma sensitivity of the system, Cs-137 and Co-60 sources were used. The gamma sensitivity was less than 1% of the neutron sensitivity.

Isotopically enriched B-10 targets were acquired to facilitate fabrication of thin-layered coatings. The materials used for the preparation of the films for neutron capture are elemental boron and boron carbide (B4C). Boron and boron carbide layers were deposited on Si wafers. Consistency of deposition was validated using XRD (to characterized layer crystalline phase) and SEM (to characterize thickness, adhesion and surface morphology). To enhance the adhesion of the B and B4C layers, the Si substrates were cleaned with alcohol, acetone and Ar plasma. Prior to the deposition of the B layers, an adhesion layer consisting of ~250 nm of Ti was deposited. The use of Ti as an adhesion layer proved to greatly increase the adhesion. The B-10 targets produced more than 40 cps when using a 50000 neutron per second source.

Isotopically enriched Li-6 layers where also deposited on Si wafers. Because of the unavailability of vendors for Li-6 targets, the target for Li deposition was prepared in house. The Li-6 rich Li_2CO_3 was melted in to a disk shape and used as a target. The material deposited through sputter deposition on to a Si wafer appears to be Li metal with an undesirable oxide layer formation on the surface. The proposed methodology to alleviate the oxide layer formation was beyond the proposed scope of the current project.

In summary: the proposed moderator block was proven to provide directional information for fast neutron detection; the optimum configuration for the moderator block was successfully modeled; and SRNL developed the capability to deposit n-reactive thin layers onto silicon material in support of custom detector fabrication.

Solid Oxide Reduction of Used Nuclear Fuel

Kyle Brinkman, Brenda Garcia-Diaz, Luke Olson and Josh Gray (SRNL)
Yanhai Du and Ken Reifsnider (USC)

This project developed an electrochemical cell using a solid oxide electrolyte for the reduction of the oxide-form Used Nuclear Fuel (UNF) from Light Water Reactors (LWRs) to yield a metallic product. The solid oxide electrolyte provided a structural material that served as a physical separator in the cell and was functionalized to serve as one of the electrodes on the surface away from the UNF electrode. The solids oxide electrode exhibited appreciable durability after molten salt exposure and demonstrated the ability to transport oxygen out of the system as evidenced by electrochemical and exhaust gas analysis. Further development of this technology is expected to result in separations processes that are less costly, more efficient and inherently safer due to UNF isolation and containment in the solid oxide reduction process.

The conventional Plutonium/Uranium Extraction (PUREX) process used to separate the constituents of UNF generates large volumes of high level waste and can be used to isolate plutonium. Non-aqueous separation methods are being developed as alternatives that do not generate liquid waste, reduce potential for Pu production and also provide benefits for process safety. Electrochemical cells for oxide reduction using molten salt electrolytes and a metallic counter electrode have been used, but require substantial amounts of electrolytes and electrodes have small surface area that limits current density. The current work outlines a novel approach using a solid oxide cell that can reduce lithium oxide at the cathode, move the oxygen ions through the solid oxide electrolyte, and oxidize them to O_2 gas at the anode. Optimization of this concept is expected to result in separations processes that are less costly, more efficient and inherently safer due to UNF isolation and containment in the solid oxide reduction process. Although initially envisioned for nuclear materials processes, the successful demonstration of this technology would be of great interest to the broader metallurgical community and to efforts aimed at rare earth materials production and recycling.

The electrochemical reduction cell was constructed to convert surrogate fuels such as CeO_2 to metallic cerium. Testing was performed with a custom Yttria Stabilized Zirconia (YSZ) solid oxide electrode which was submerged in a LiCl-KCl molten salt electrolyte with Li_2O additives along with the CeO_2 surrogate pellets in a graphite electrode basket. A platinum quasi-reference electrode was employed for interpretation of electrochemical data. The solid oxides, molten salt electrolytes, and electrodes were analytically characterized using X-ray diffraction as well as SEM-EDS examining microstructure and chemical composition. The mechanical properties of YSZ solid oxide electrodes were studied before and after exposure to molten salt at elevated temperature (650^{o}C) at the University of South Carolina (USC).

Figure 1a) summarizes the mechanical property testing of YSZ solid oxide tubes before and after exposure to the high temperature molten salt. Compressive testing on tubular specimens was performed with Figure 1a) displaying the compressive force versus displacement. Samples before exposure to molten salt (green lines) typically have 3 peaks, indicating the YSZ tubes had small elastic features. However, the samples tested after molten salt exposure exhibited 1-2 peaks, which indicates brittle/glassy behavior. Molten salt exposure made the tubes stronger but brittle at room temperature due to microstructure modifications at the grain boundary as seen in Figure 1b). Further testing is required for long term durability predictions since room temperature strength cannot accurately represent high temperature strength.

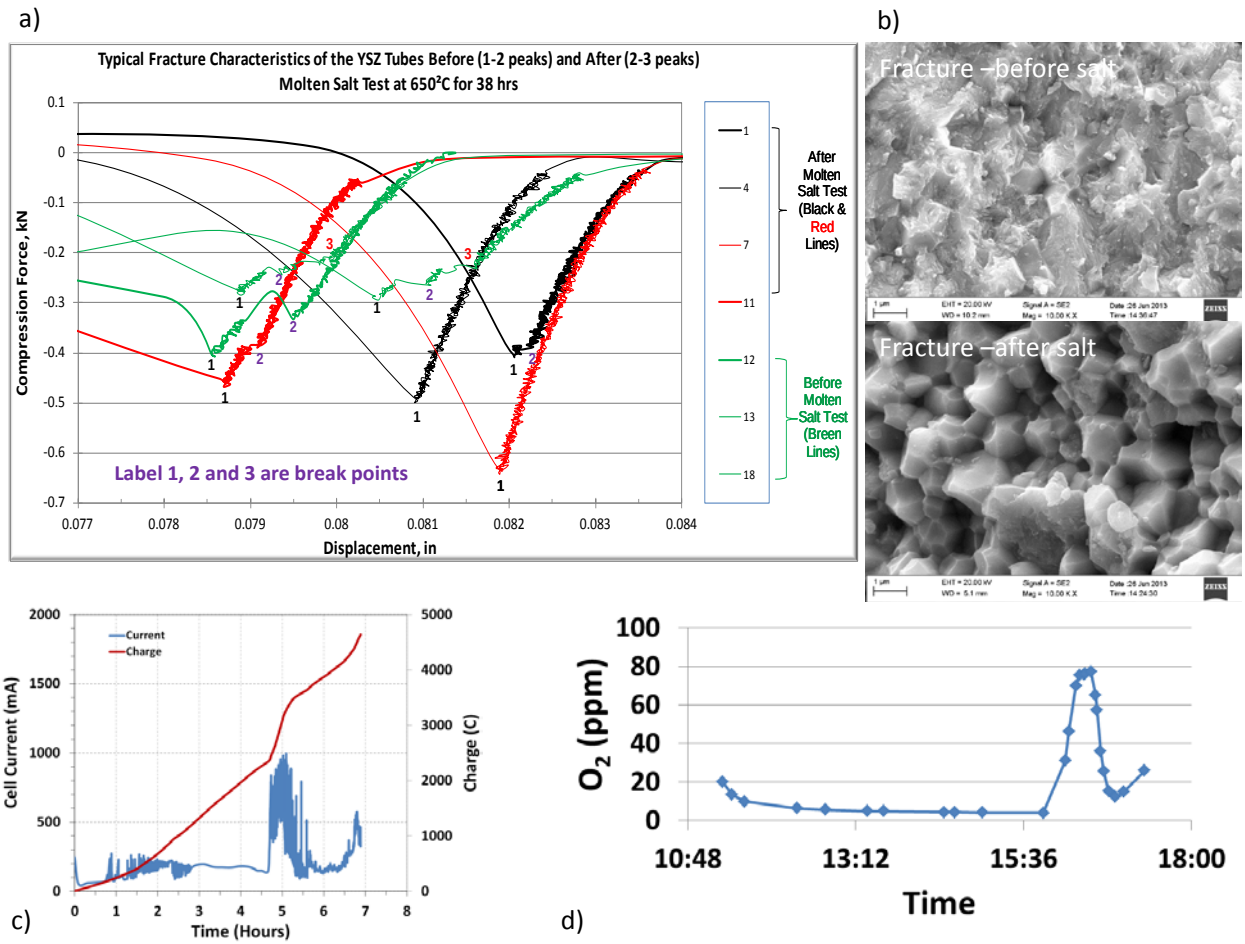

Figure 2. a) Force (kN) versus displacement (in) fracture characteristics of YSZ tubes before and after molted salt exposure and b) SEM fracture surfaces of YSZ tubes before and after salt exposure 650°C 1 hour c) reduction of the oxide during electrolysis d) evolution of oxygen during the electrolysis experiment.

Figure 1 part c) and d) show different aspects of the electrolysis experiment to reduce CeO_2. Figure 1c) shows the current and charge passed during the reduction experiment. A large increase in the current near 4.5 hours showed very strong reduction of the CeO_2. This may correspond to a slow incubation period up to 4.5 hours where the passive layer is slowly reduced followed by a more rapid reduction as the electrode area increases. Figure 1d) shows that approximately 4.5 hours after the start of the electrolysis experiment oxygen was being produced at the cathode. The oxidation appears to have occurred during the time when there is a large increase in current. This incubation time may be needed in order to develop percolation of reduced Ce to contact the electrode since CeO_2 has relatively low electronic conductivity at these conditions. This issue may be addressed with electrode microstructure optimization in future work.

These experiments clearly showed that oxides could be electrochemically reduced in molten salts at high temperature with a solid oxide cathode. The CeO_2 surrogate electrode was partially reduced during the experiment as confirmed by electrochemical data and SEM-EDS. It was shown that O_2 was produced by the electrolysis reaction after an electronic conductive network in the anode electrode system was achieved after an initial incubation time. The development of solid oxide electrodes for reduction of nuclear fuel to a metallic state is therefore a very promising application of solid oxide membranes that warrants further study and attention.